International Journal of Solids and Structures 50 (2013) 1562–1582

Contents lists available at SciVerse ScienceDirect

International Journal of Solids and Structures

journal homepage: www.elsevier.com/locate/ijsolstr

Mode mixity and size effect in V-notched structures

P. Cornetti *, A. Sapora, A. Carpinteri

Department of Structural, Geotechnical and Building Engineering, Politecnico di Torino, Torino, Italy

ARTICLE INFO

Article history:
Received 12 November 2012
Received in revised form 7 January 2013
Available online 8 February 2013

Keywords:
Sharp notches
Mode mixity
Size effect
Finite fracture mechanics

ABSTRACT

Aim of the present paper is twofold. On one hand, we apply the Finite Fracture Mechanics criterion to address the problem of a V-notched structure subjected to a mixed-mode loading, i.e. we provide a way to determine the direction and the load at which a crack propagates from the notch tip. On the other hand, we make use of the formalism recently introduced by Hills & Dini [Hills D.A., Dini D. Characteristics of the process zone at sharp notch roots. International Journal of Solids and Structures 48:2177–2183] and express the critical conditions in terms of the notch driving force plus a suitable definition of the notch mode mixity. Weight functions of the stress intensity factors for V-notch-emanated cracks available in the literature allow us to implement the fracture criterion proposed in an almost completely analytical manner. Dimensionless values of the critical generalized stress intensity factors are tabled accurately in order to be of help in engineering practice. We then derive some theoretical implications from the obtained results, highlighting the size effect for a V-notched structure under mixed-mode loading and the differences between the structural behaviors of cracked and notched geometries. Some example problems, highlighting the capabilities of the model, conclude the paper.

1. Introduction

The development of suitable fracture criteria for brittle (isotropic or orthotropic) materials containing V-notches or multimaterial interfaces is a problem of primary concern in order to control fracture onset phenomena taking place in mechanical components, composite materials and electronic devices (e.g. Yosibash et al., 2003; Barroso et al., 2012). As well-known, the singularity of the stress field in the vicinity of the notch tip makes the problem non-trivial.

Concerning re-entrant corners in homogeneous media subjected to mode I loadings, since the pioneering paper by Carpinteri (1987) a good correlation has been found between the critical value of the generalized stress intensity factor (i.e. the generalized fracture toughness) and the failure loads. Theoretical models to relate the generalized fracture toughness to material tensile strength, fracture toughness and re-entrant corner amplitude have been set by a number of researchers, e.g. Seweryn (1994), Lazzarin and Zambardi (2001), Leguillon (2002) and Carpinteri et al. (2008).

Fewer contributions are available for what concerns more complex loading conditions or out-of-plane effects (Berto et al., 2011). As regards mixed mode loadings, we can cite the papers by Seweryn et al. (1997), Seweryn and Lukaszewicz (2002), Yosibash et al. (2006) and Gómez et al. (2009), all of them representing the extension of the corresponding fracture criteria for mode I loading. Here we provide the generalization of the results obtained in Carpinteri et al. (2008) to mixed mode problems. The proposed approach (as well as the ones previously cited) is based on the assumption that the region around the corner dominated by the singular stress field is large compared to intrinsic flaw sizes, inelastic zones or fracture process zone sizes. This hypothesis is the analogous of small-scale yielding in Linear Elastic Fracture Mechanics (LEFM).

While in LEFM there is a direct connection between the Stress Intensity Factors (SIFs) and the strain energy release rate (i.e. Irwin's relationship), this relation is missing in the case of notches, so that correlating fracture initiations with critical values of the stress intensity (Carpinteri, 1987; Dunn et al., 1997a) could appear questionable. However, the recently introduced Finite Fracture Mechanics (FFM) criterion has shown this is not the case (Leguillon, 2002; Carpinteri et al., 2008). In fact, under the assumption of a finite crack extension at fracture initiation, it is possible to prove a relation between the Generalized Stress Intensity Factors (GSIFs) and the energy released when a crack appears at the V-notch tip.

Concerning FFM and without claiming to be exhaustive, here we want just to note that in recent years it has proved to be successful in addressing several structural problems, spanning from V-notched to porous structures (Leguillon and Piat, 2008), composites (Hebel et al., 2010; Mantič, 2009; Camanho et al., 2012) or interface problems (Weißgraeber and Becker, 2011; Cornetti

* Corresponding author. Tel.: +39 0110904901; fax: +39 0110904899.
E-mail address: pietro.cornetti@polito.it (P. Cornetti).

0020-7683/$ - see front matter © 2013 Elsevier Ltd. All rights reserved.
http://dx.doi.org/10.1016/j.ijsolstr.2013.01.026

et al., 2012). Furthermore FFM has been able to predict the size effect arising in several contexts, as, for instance, three point bending cracked and plain concrete beams (Cornetti et al., 2006), holed PMMA plates (Hebel and Becker, 2008), blunt notched ceramic specimens (Leguillon et al., 2007; Carpinteri et al., 2011).

Beyond addressing the problem of V-notched structures under mixed-mode loadings according to the FFM criterion given in Cornetti et al. (2006), the present paper is original under other aspects. Firstly, we take advantage of the formalism introduced in Hills and Dini (2011) where a description of the asymptotic stress field at the notch tip has been provided in terms of new mechanical quantities (i.e. the notch driving force and the mode mixity length) with integer physical dimensions; such a description looks more rational than the traditional one in terms of the GSIFs, characterized by non-integer physical dimensions. The present work can be seen somehow as the fracture mechanics analysis counterpart of the plastic zone shape analysis investigated in Hills and Dini (2011). A novel definition of mode mixity is given, clearly highlighting that for notched structures the failure load and crack deflection depend also on the material brittleness in addition to the GSIFs ratio. In this sense, the mechanical behavior of V-notched structures strongly differs from that of cracked structures.

A second original point, with respect to the FFM approach proposed in Yosibash et al. (2006), is that the problem is handled in an analytical way. By exploiting the weight functions provided by Beghini et al. (2007), the determination of the direction of the V-notch emanated crack and of the crack onset load can be cast in a standard minimization-under-constraint problem that can be solved by means of the Lagrange multiplier technique.

A third original aspect is the analysis of the size effect. Since the paper by Carpinteri (1987), it is well-known that, for mode I loadings, the size effect upon strength is represented by a power law whose (negative) exponent is given by the power of the (mode I) stress singularity. On the other hand, here we prove that, for the general case of mixed-mode loadings, the size effect is given by a curve which is intermediate between two power laws: the former one, holding at small scales, with exponent equating the mode II singularity; the latter one, valid for large scales, with exponent equating the mode I singularity. Furthermore, the present approach allows one also to discriminate between the geometries where the mode II contribution is negligible and the configurations where it must be taken into account. This is another important aspect of the problem since it is often stated that the mode II contribution is negligible, especially for large notch opening angle (e.g. 90°) when the anti-symmetric singularity is weak (see e.g. Dunn et al., 1997b). Although this statement can be true in a large number of cases, there are also geometries where the mode II contribution is relevant, as we will show in the end of the paper.

The plan of the paper is as follows. In Section 2 we revisit Williams analysis according to the paper by Hills and Dini (2011) and, by means of dimensional analysis, we find some general rules that will act as guidelines for the subsequent analysis. In Section 3 the SIFs for a V-notch emanated crack are derived starting from suitable weight functions available in the literature. In Section 4 the FFM criterion is applied to the problem at hand and the results are presented in terms of the notch driving force in Section 5 and in terms of the GSIFs in Section 6. In Section 7, the average stress criterion is recalled for the sake of comparison and the size effect is deeply investigated in Section 8. Finally, Section 9 presents some example problems characterized by a unique relevant geometrical length: in such a case we prove that, for a given loading set, a one-to-one correspondence exists between the mode mixity and the brittleness number introduced by Carpinteri (1980, 1981, 1982), which thus plays a crucial role also in the analysis of V-notched structures subjected to mode I plus mode II loadings.

2. Stress field, dimensional analysis and mode mixity

Let us consider a re-entrant corner in an infinite homogeneous elastic medium with a polar coordinate system (r,ϑ) centred at the V-notch tip (see Fig. 1(a). After Williams (1952) the asymptotical stress field is given by:

$$\sigma_{rr} = \frac{K_I^*}{(2\pi r)^{1-\lambda_I}} f_{rr}^{I}(\vartheta,\omega) + \frac{K_{II}^*}{(2\pi r)^{1-\lambda_{II}}} f_{rr}^{II}(\vartheta,\omega) \tag{1a}$$

$$\sigma_{\vartheta\vartheta} = \frac{K_I^*}{(2\pi r)^{1-\lambda_I}} f_{\vartheta\vartheta}^{I}(\vartheta,\omega) + \frac{K_{II}^*}{(2\pi r)^{1-\lambda_{II}}} f_{\vartheta\vartheta}^{II}(\vartheta,\omega) \tag{1b}$$

$$\tau_{r\vartheta} = \frac{K_I^*}{(2\pi r)^{1-\lambda_I}} f_{r\vartheta}^{I}(\vartheta,\omega) + \frac{K_{II}^*}{(2\pi r)^{1-\lambda_{II}}} f_{r\vartheta}^{II}(\vartheta,\omega) \tag{1c}$$

where K_I^* and K_{II}^* are the GSIFs in mode I (symmetrical) and mode II (anti-symmetrical) loading conditions respectively, λ_I and λ_{II} are the well-known Williams' eigenvalues and the functions f_{ij} are the angular shape functions (i.e. the eigenvectors), whose explicit expressions are reported in Appendix A. Both eigenvalues and eigenvectors depend on the notch opening angle ω. The values of the eigenvalues are reported in Table 1 for discrete values of the re-entrant corner amplitude. Note that the definition of the GSIFs is somewhat arbitrary, depending on the choice of the normalization factor, here taken equal to $(2\pi)^{1-\lambda_i}$ as in Seweryn (1994) but equal to 1 or to $\sqrt{2\pi}$ in other papers (e.g. Yosibash et al. (2006) and Lazzarin and Zambardi (2001), respectively). As we shall see later, the advantage of such a choice is that the critical value of the mode I GSIF continuously varies from the material tensile strength to the material fracture toughness as the re-entrant corner amplitude diminishes from 180° (flat edge) to 0° (cracked plate).

We can give Eq. (1) a different, dimensionless formulation by applying Buckingham Π-theorem. In fact, we can state that the generic stress component σ_{ij} (where i and j are equal either to r or to ϑ) depends on five quantities: $K_I^*, K_{II}^*, r, \vartheta$ and ω. In the static field, only two fundamental dimensions appear: length [L] and force [F]. Being dimensionally independent, we can choose as fundamental quantities the two GSIFs. The Π-theorem allows us to assert that the dimensionless stresses depend only on three dimensionless quantities by means of the functions g_{ij}:

$$\frac{\sigma_{ij}}{G_0} = g_{ij}\left(\frac{r}{d_0},\vartheta,\omega\right) \tag{2}$$

with:

$$G_0 = \left(K_I^*\right)^{-\frac{1-\lambda_{II}}{\lambda_{II}-\lambda_I}}\left(K_{II}^*\right)^{\frac{1-\lambda_I}{\lambda_{II}-\lambda_I}}, \quad d_0 = \left(\frac{K_I^*}{K_{II}^*}\right)^{\frac{1}{\lambda_{II}-\lambda_I}} \tag{3}$$

where the exponents of the GSIFs have been determined by imposing that the product $\left(K_I^*\right)^{\alpha} \times \left(K_{II}^*\right)^{\beta}$ has the dimension of a stress and of a length respectively. Note that such a dimensionless formulation is not possible for a crack, when the mode I and mode II SIFs have the same physical dimension and are not, therefore, dimensionally independent. The inverse of Eq. (3) reads:

$$K_I^* = G_0 d_0^{1-\lambda_I}, \quad K_{II}^* = G_0 d_0^{1-\lambda_{II}} \tag{4}$$

On the basis of Eq. (2), we can give the following dimensionless form to Eq. (1):

$$\frac{\sigma_{ij}}{G_0} = \frac{f_{ij}^{I}(\vartheta,\omega)}{(2\pi r/d_0)^{1-\lambda_I}} + \frac{f_{ij}^{II}(\vartheta,\omega)}{(2\pi r/d_0)^{1-\lambda_{II}}} \tag{5}$$

Note that in Eqs. (3)–(5) we assumed that both the GSIFs are positive. While the condition $K_I^* > 0$ is a physical one, the condition $K_{II}^* > 0$ has been introduced only for sake of simplicity and will be removed later.

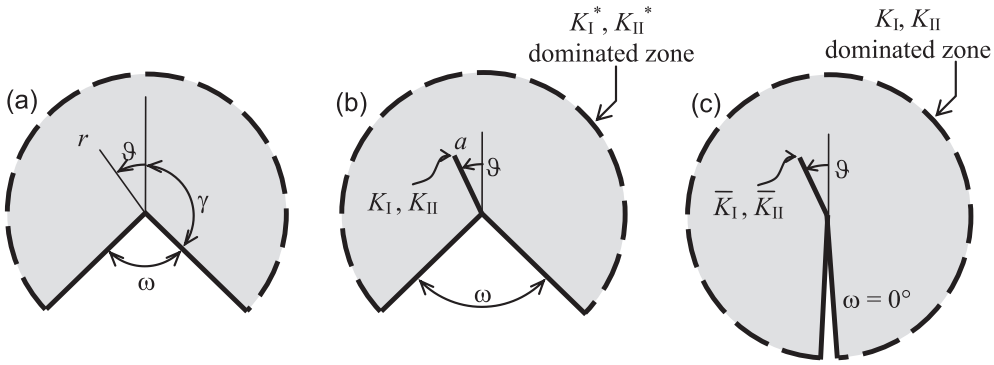

Fig. 1. Polar reference system at the tip of a V-notch (a); V-notch emanated crack within the GSIFs dominated stress field region (b); kinked crack problem (c).

Table 1
Eigenvalues and parameters depending only on the notch opening angle ω.

ω [°]	λ_I	λ_{II}	ξ	ϑ_{IIc} [°]	η
0	0.5	0.5	1	75.6	0.811
20	0.50043	0.56201	0.9853	71.2	0.849
30	0.50145	0.59819	0.9856	68.2	0.870
40	0.50349	0.63818	0.9868	65.7	0.887
50	0.50693	0.68230	0.9886	63.3	0.901
60	0.51222	0.73090	0.9910	60.9	0.910
70	0.51985	0.78444	0.9940	58.5	0.913
80	0.53040	0.84344	0.9975	56.3	0.912
90	0.54448	0.90853	1.0017	54.0	0.904
100	0.56284	0.98048	1.0063	51.8	0.890

The nicely symmetric Eq. (5) was given in Hills and Dini (2011). Instead of depending on the two GSIFs with non-integer physical dimensions, the stress field expressed through Eq. (5) depends on the two quantities G_0 and d_0, which have the (integer) physical dimensions of a stress and of a length, respectively. In our opinion, the description of the stress state in terms of (G_0,d_0) instead of (K_I^*, K_{II}^*) seems to be more *rational*. While in terms of (K_I^*, K_{II}^*) both the GSIFs are proportional to the applied loads, in terms of (G_0,d_0) the information about the load intensity is condensed in G_0, which acts as a *notch driving force* (Hills and Dini, 2011) and controls the magnitude of the applied load. On the other hand d_0, which is independent of the load magnitude but dependent on the load configuration, determines the mode mixity; thus, hereafter we will refer to d_0 as the *mode mixity length*. Furthermore, since $1-\lambda_I > 1-\lambda_{II}$, from Eq. (5) it is evident that the mode I term is dominant close to the notch tip ($r \ll d_0$), whereas the mode II term dominates at larger distances ($r \gg d_0$). Thus small d_0 denotes a prevailing mode II loading, whereas large d_0 denotes a prevailing mode I loading.

Let us now turn the attention to the attainment of critical conditions. We want to apply dimensional analysis to derive the general form a fracture criterion for mixed-mode V-notched structures must possess. To this aim, we assume that the conditions for incipient failure are satisfactorily described by two material parameters, i.e. the fracture toughness K_{Ic} and tensile strength σ_u. Assuming a brittle structural behavior, the V-notched structure will behave linear-elastically up to a critical load level, when a crack will appear at the V-notch tip (Fig. 1(b). The brittleness assumption allows us to work only with the asymptotic stress field (Eq. (1)). These physical hypotheses can be mathematically translated into:

$$\left.\begin{matrix} G_{0f} \\ \vartheta_c \end{matrix}\right\} = f(K_{Ic}, \sigma_u, d_0, \omega) \tag{6}$$

In Eq. (6) and henceforth, f denotes a generic dependence on some variables and not a specific function. That is, both the failure load (expressed either as the critical value of the notch driving force G_{0f} or, equivalently, as the critical value of the mode I GSIF K_{If}^*) and the direction of crack propagation ϑ_c, i.e. the crack deflection with respect to the notch bisector, depend on fracture toughness, tensile strength, mode mixity length and notch opening angle. Choosing now as fundamental quantities K_{Ic} and σ_u, a straightforward application of Buckingham theorem allows us reducing the dependency to two dimensionless parameters:

$$\left.\begin{matrix} G_{0f}/\sigma_u \\ \vartheta_c \end{matrix}\right\} = f\left(\frac{d_0}{l_{ch}}, \omega\right) \text{ or } \left.\begin{matrix} K_{If}^*/\left(\sigma_u l_{ch}^{1-\lambda_I}\right) \\ \vartheta_c \end{matrix}\right\} = f\left(\frac{d_0}{l_{ch}}, \omega\right) \tag{7}$$

where $l_{ch} = (K_{Ic}/\sigma_u)^2$ is the well known Irwin characteristic length. Eq. (7) clearly shows that the failure load and the crack initiation direction depend on the ratio d_0/l_{ch}; or, equivalently, that the *effective* mode mixity is defined by the ratio d_0/l_{ch}. It means that the mode mixity at incipient failure does not depend only on the loading geometry, but also on the material brittleness through l_{ch}: for a given GSIFs ratio (i.e. for a given d_0), failure will be more in mode I for more brittle materials (small l_{ch}) and more in mode II for less brittle materials. This is a key difference with respect to the crack case (Fig. 1(c)), where the analogous to Eq. (7) reads:

$$\left.\begin{matrix} K_{If}/K_{Ic} \\ \vartheta_c \end{matrix}\right\} = f\left(\frac{K_{II}}{K_I}\right) \tag{8}$$

that is, the mode mixity does not depend on the material, being simply the ratio between the SIFs. Thus, dimensional analysis shows that, for a given SIF ratio, the direction of crack kinking for a crack in an infinite plate is the same for any (brittle) material; on the other hand, the direction of a crack stemming from a re-entrant corner does depend on the material (beyond on the ratio between the GSIFs). A deeper analysis of this non-trivial feature will be given in the following sections.

Before proceeding, some comments are useful. Firstly, it is worth highlighting the analogy between these results and the ones obtained in Hills and Dini (2011). While, within a plasticity analysis framework, Hills and Dini (2011) pointed out that the shape of the plastic zone depends on the load level for a V-notch whereas it does not for a crack, within the present brittle fracture analysis context, we show that for a re-entrant corner, varying the material brittleness, the fracture load varies and, consequently, also the crack propagation direction changes.

Secondly, we must observe that, although the description of the state of stress (as well as of the attainment of critical conditions) at the vertex of a V-notch is more elegant in terms of G_0 and d_0, such a description does not work when one of the three quantities K_I^*, K_{II}^*, ω is null, i.e. it does not work in pure mode II, in pure mode I and for cracked geometries. In fact, as is evident from Eq. (3), in these extreme cases, G_0 and d_0 are either zero or infinite for any applied load and therefore unable to describe the stress state.

Therefore, to have a general description of the problem, it may be more useful to keep on working with the GSIFs (K_I^*, K_{II}^*) instead of G_0 and d_0. However, for what concerns the mode mixity and in order to preserve the advantages of both the approaches, we propose the following definition of mode mixity:

$$\psi = \arctan\left[\left(\frac{d_0}{l_{ch}}\right)^{-(\lambda_{II}-\lambda_I)}\right] = \arctan\frac{K_{II}^* l_{ch}^{\lambda_{II}-\lambda_I}}{K_I^*} \tag{9}$$

In fact, by raising d_0 to $(\lambda_{II} - \lambda_I)$ we remove the indeterminateness in the crack case, while taking the arc tangent we can describe mode II without having a parameter going to infinity: $\psi = 0$ denotes pure mode I loading conditions whereas $\psi = \pi/2$ denotes pure mode II loading conditions. Even more important, the given definition of mode mixity clearly shows that it depends on the material through l_{ch} except in the three extreme cases of pure mode I $(K_{II}^* = 0 \Rightarrow \psi \equiv 0)$, pure mode II $(K_I^* = 0 \Rightarrow \psi \equiv \pi/2)$, and cracked geometries ($\lambda_I = \lambda_{II} = 1/2$, $\psi = \arctan\ (K_{II}/K_I)$). In the following, we will refer to ψ as *the mode mixity angle*, or, more simply, as the mode mixity. Moreover, it is worth observing that using as a definition of mode mixity the last member in Eq. (9), one can remove the assumption of positive K_{II}^*: it simply means that, if $K_{II}^* > 0$, then $0 < \psi < \pi/2$, while if $K_{II}^* < 0$, then $-\pi/2 < \psi < 0$. Hence mode II conditions are met if $\psi = \pm\pi/2$.

To summarize the results of the present section, we can state that, by means of dimensional analysis, we have been able to derive the general form of a fracture propagation criterion applied to re-entrant corners under mixed mode loading as:

$$\vartheta_c = f_1(\psi,\omega) \quad \text{and}$$
$$G_{0f}/\sigma_u = f_2(\psi,\omega) \quad \text{or} \quad K_{If}^*/\left(\sigma_u l_{ch}^{1-\lambda_I}\right) = f_3(\psi,\omega) \tag{10}$$

In the following sections we will provide the values of functions f_1 to f_3 according to a specific fracture criterion, i.e. FFM.

3. Stress intensity factors for a V-notch emanated crack

In order to apply the FFM criterion, we need to evaluate the energy necessary for the abrupt appearance of a finite length crack at the notch tip. This quantity can be easily computed if the SIFs K_I and K_{II} of a crack at the notch vertex are known. To this aim, we begin noticing that, if the crack occurs within the GSIFs dominated stress field, the SIFs depend only on the GSIFs, crack direction ϑ, crack length a and notch opening angle ω (see Fig. 1(b)). Once more, a straightforward application of the Π theorem (as well as the principle of effect superposition) shows that this dependency must take the following form (Li and Zhang, 2006):

$$K_I = \mu_{11}(\vartheta,\omega)K_I^* a^{\lambda_I - 1/2} + \mu_{12}(\vartheta,\omega)K_{II}^* a^{\lambda_{II}-1/2} \tag{11a}$$
$$K_{II} = \mu_{21}(\vartheta,\omega)K_I^* a^{\lambda_I - 1/2} + \mu_{22}(\vartheta,\omega)K_{II}^* a^{\lambda_{II}-1/2} \tag{11b}$$

This formula is particularly interesting since it encompasses the case of pure mode I loaded V-notches and the case of the kinked crack problem. In the former case, the emanated crack grows along the notch bisector ($\vartheta = 0$); hence K_{II} is zero and K_I simplifies into:

$$K_I = \mu_{11}(\omega)K_I^* a^{\lambda_I - 1/2} \tag{12}$$

Eq. (12) dates back to Hasebe and Iida (1978); highly accurate values of the dimensionless coefficient $\mu_{11}(\omega)$ have been provided in Philipps et al. (2008) and Livieri and Tovo (2009). In the latter case $\lambda_I = \lambda_{II} = 1/2$; thus Eq. (11) becomes (see, e.g., Melin, 1994):

$$\overline{K}_I = \mu_{11}(\vartheta,\omega=0)K_I + \mu_{12}(\vartheta,\omega=0)K_{II} \tag{13a}$$
$$\overline{K}_{II} = \mu_{21}(\vartheta,\omega=0)K_I + \mu_{22}(\vartheta,\omega=0)K_{II} \tag{13b}$$

which provide the SIFs $\overline{K}_I, \overline{K}_{II}$ at the tip of the (secondary) crack, kinked with respect to the main (primary) crack, with SIFs K_I,K_{II} (see Fig. 1(c)). Note that for the kinked crack case the dependence on the crack length a disappears (as long as the secondary crack lies in the K_I,K_{II} dominated region, i.e. the length of the secondary crack is much smaller than the one of the primary crack).

While the dimensionless μ_{ij} parameters in Eq. (13), i.e. for $\omega = 0$, can be found tabulated with great accuracy in Melin (1994), their values for a generic notch opening angle ω are not available. Nevertheless, they can be obtained by exploiting the results provided by Beghini et al. (2007), where the SIFs for a pair of forces per unit thickness (either normal, P, or tangential, T) acting on the faces of a V-notch emanated crack are given, see Fig. 2. Beghini et al. (2007) evaluated such SIFs for several ω and ϑ values by proper finite element computations and found that an accurate analytical expression of the SIFs can be given as:

$$K_I = \frac{P\sqrt{2}}{\sqrt{\pi(a-r)}}\left\{1 + \frac{a-r}{a}\left[B^{I\sigma}(\vartheta,\omega) + \frac{T}{P}B^{I\tau}(\vartheta,\omega)\right]\right\} \tag{14a}$$
$$K_{II} = \frac{T\sqrt{2}}{\sqrt{\pi(a-r)}}\left\{1 + \frac{a-r}{a}\left[B^{II\tau}(\vartheta,\omega) + \frac{P}{T}B^{II\sigma}(\vartheta,\omega)\right]\right\} \tag{14b}$$

where r is the distance from the notch tip where the pairs of forces act. The form of expressions (14) was chosen such that, for $r \to a$, the terms in curly brackets tend to unity and the SIFs are given by the well-known asymptotic values for a pair of forces acting close to the crack tip, represented by the terms outside the curly brackets in Eq. (14). Note that only for this asymptotic case ($r \to a$), the modes are uncoupled, i.e. P causes only K_I ($K_{II} = 0$) and T yields only K_{II} ($K_I = 0$). The coefficients $B^{I\sigma}$, $B^{I\tau}$,$B^{II\sigma}$ and $B^{II\tau}$ are numerical coefficients depending on the notch opening angle ω and crack orientation ϑ. They have been computed as best fit parameters, i.e. imposing that Eq. (14) fit the numerical values obtained by finite element analyses. Their expressions are provided in Beghini et al. (2007) as truncated trigonometric and power series expansions of ϑ and ω, respectively; their range of validity are $-72° < \vartheta < +72°$ and $18° < \omega < 144°$.

Eqs. (14) can be used as weight functions, i.e. if the crack faces are loaded by a continuous stress distribution $\sigma_{\vartheta\vartheta}(r)$,$\tau_{r\vartheta}(r)$ along the crack faces ($0 < r < a$), the SIFs are given upon substitution in Eq. (14) of the concentrated forces P and T by $[\sigma_{\vartheta\vartheta}(r)\,dr]$ and $[\tau_{r\vartheta}(r)\,dr]$, respectively, and finally upon integration:

$$K_I = \int_0^a \frac{\sqrt{2}}{\sqrt{\pi(a-r)}}\left\{\left[1 + \frac{a-r}{a}B^{I\sigma}\right]\sigma_{\vartheta\vartheta}(r) + \frac{a-r}{a}B^{I\tau}\tau_{r\vartheta}(r)\right\}dr \tag{15a}$$
$$K_{II} = \int_0^a \frac{\sqrt{2}}{\sqrt{\pi(a-r)}}\left\{\left[1 + \frac{a-r}{a}B^{II\tau}\right]\tau_{r\vartheta}(r) + \frac{a-r}{a}B^{II\sigma}\sigma_{\vartheta\vartheta}(r)\right\}dr \tag{15b}$$

The SIFs for a notch emanated crack within the GSIFs-dominated stress field can now be obtained by a standard application of the principle of effect superposition. In fact, as outlined in Fig. 3 (where, for the sake of simplicity, only mode I loading has been considered), the SIFs for a generic remote loading (Fig. 3(a)) coincide with the ones of the geometry where the crack faces are loaded by the stress field occurring if crack were closed

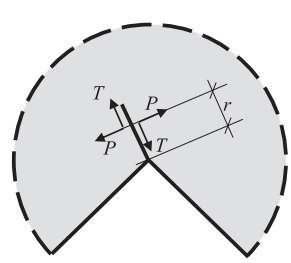

Fig. 2. V-notch emanated crack loaded by a pair of normal (P) and tangential (T) forces acting at a distance r from the notch tip.

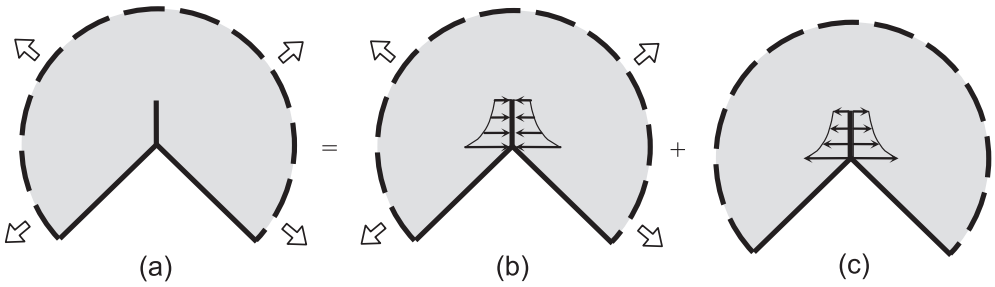

Fig. 3. Principle of effect superposition to compute the SIF of a V-notch emanated crack. The stress field in (b) is the one occurring ahead of the V-notch if no crack were present. Therefore the SIF at the tip of the crack is zero in configuration (b) and the SIFs for the loading conditions (a) and (c) must coincide. For the sake of simplicity, the figure refers only to mode I loading.

(Fig. 3(c)). Consequently, the SIFs for a V-notch emanated crack (Fig. 1(b)) is obtained by replacing the stress field (1) into Eq. (15). Integration can be performed in closed form and expressions (11) are recovered along with the following analytical expressions for the dimensionless μ coefficients:

$$\mu_{11} = \frac{2^{\lambda_I - 1/2}}{\pi^{3/2-\lambda_I}} \Big\{ f^{I}_{\vartheta\vartheta}(\vartheta,\omega)[\beta(\lambda_I,1/2) + B^{I\sigma}(\vartheta,\omega)\beta(\lambda_I,3/2)] + f^{I}_{r\vartheta}(\vartheta,\omega)B^{I\tau}(\vartheta,\omega)\beta(\lambda_I,3/2)\Big\} \tag{16a}$$

$$\mu_{12} = \frac{2^{\lambda_{II} - 1/2}}{\pi^{3/2-\lambda_{II}}} \Big\{ f^{II}_{\vartheta\vartheta}(\vartheta,\omega)[\beta(\lambda_{II},1/2) + B^{I\sigma}(\vartheta,\omega)\beta(\lambda_{II},3/2)] + f^{II}_{r\vartheta}(\vartheta,\omega)B^{I\tau}(\vartheta,\omega)\beta(\lambda_{II},3/2)\Big\} \tag{16b}$$

$$\mu_{21} = \frac{2^{\lambda_I - 1/2}}{\pi^{3/2-\lambda_I}} \Big\{ f^{I}_{\vartheta\vartheta}(\vartheta,\omega)B^{II\sigma}(\vartheta,\omega)\beta(\lambda_I,3/2) + f^{I}_{r\vartheta}(\vartheta,\omega)[\beta(\lambda_I,1/2) + B^{II\tau}(\vartheta,\omega)\beta(\lambda_I,3/2)]\Big\} \tag{16c}$$

$$\mu_{22} = \frac{2^{\lambda_{II} - 1/2}}{\pi^{3/2-\lambda_{II}}} \Big\{ f^{II}_{\vartheta\vartheta}(\vartheta,\omega)B^{II\sigma}(\vartheta,\omega)\beta(\lambda_{II},3/2) + f^{II}_{r\vartheta}(\vartheta,\omega)[\beta(\lambda_{II},1/2) + B^{II\tau}(\vartheta,\omega)\beta(\lambda_{II},3/2)]\Big\} \tag{16d}$$

where $\beta(a,b)$ is the well-known Euler beta function, defined as:

$$\beta(a,b) = \int_0^1 t^{a-1}(1-t)^{b-1}\mathrm{d}t \tag{17}$$

Analogously to what we did for the stress field, also the SIFs can be expressed in terms of the new quantities (G_0,d_0) instead of (K^*_I, K^*_{II}), as occurs in Eq. (11). Substituting Eq. (4) into Eq.(11) yields:

$$\frac{K_I}{G_0\sqrt{d_0}} = \mu_{11}\left(\frac{a}{d_0}\right)^{\lambda_I - 1/2} + \mu_{12}\left(\frac{a}{d_0}\right)^{\lambda_{II} - 1/2} \tag{18a}$$

$$\frac{K_{II}}{G_0\sqrt{d_0}} = \mu_{21}\left(\frac{a}{d_0}\right)^{\lambda_I - 1/2} + \mu_{22}\left(\frac{a}{d_0}\right)^{\lambda_{II} - 1/2} \tag{18b}$$

Eqs. (18) show that the SIFs of the crack are affected mainly by the mode I V-notch loadings if the crack is short, i.e. as $a \ll d_0$, whereas the mode II V-notch loading effects are dominant for relatively long cracks, i.e. when $a \gg d_0$.

For what concerns the precision of the weight functions, Beghini et al. (2007) state that Eq. (15) allow to obtain the SIFs for a generic remote loading with accuracy usually better than 1%. We further compared the values of μ_{11} for $\vartheta = 0$ (providing the SIF for a crack along the bisector under mode I loading, see Eq. (12)) with the accurate values provided by Philipps et al. (2008) for different ω values and found that the relative difference is always less than 1.2%. A further final check will be provided in the following section.

4. Coupled criterion

It is well known that both strength criteria and LEFM fail in predicting the failure load causing fracture propagation from a V-notch. In fact, the stress field given by Eq. (1) is singular and strength criteria provide a vanishing failure load. On the other hand, the SIFs provided by Eq. (11) vanish as the crack length a tends to zero and, consequently, LEFM provides an infinite failure load. These shortcomings can be overcome by resorting to Finite Fracture Mechanics (Leguillon, 2002; Cornetti et al., 2006), which couples the stress and energy approaches. Following the FFM approach proposed by Cornetti et al. (2006), a crack propagates by a finite crack extension Δ if the following two inequalities are satisfied:

$$\begin{cases} \int_0^\Delta \mathcal{G}(a')\mathrm{d}a' \geqslant \mathcal{G}_c\Delta \\ \int_0^\Delta \sigma_{\vartheta\vartheta}(r)\mathrm{d}r \geqslant \sigma_u\Delta \end{cases} \tag{19}$$

where σ_u is the material tensile strength and $\mathcal{G}_c$ is the fracture energy, related to the material fracture toughness by the well-known relation $\mathcal{G}_c = K^2_{Ic}/E'$, where $E' = E/(1-\nu^2)$, E being the Young's modulus and ν the Poisson's coefficient.

The FFM criterion (19) can be regarded as a coupled Griffith–Rankine non-local failure criterion: the former inequality is an energy balance, whereas the latter is an (average) stress requirement for crack to propagate. It means that fracture is energy driven, but a sufficiently high stress field must act at the crack tip to trigger crack propagation. It is worth observing that, in the present case (which is the usual one, i.e. a positive geometry), the strain energy release rate function $\mathcal{G}(a')$ is monotonically increasing since the SIFs increase along with the crack length (see Eq. (11)) while the stress $\sigma_{\vartheta\vartheta}(r)$ is monotonically decreasing with the distance r (see Eq. (1)) from the notch tip (as far as both the modes provide a stress singularity, i.e. for a notch opening angle less than about 102.6°). This means that the lowest failure load (i.e. the actual one) is attained when the two inequalities are substituted by the two corresponding equations. In fact the first inequality is satisfied for crack steps larger than a threshold value, thus providing a lower bound for the set of admissible Δ-values; on the contrary, the second inequality is satisfied for crack advancements smaller than a certain value, thus providing an upper bound. For low load values, the upper bound is smaller than the lower bound and, consequently, the set of admissible Δ-values is empty. As the external load increases, the upper bound increases and the lower bound decreases till a load value is met (i.e. the failure load) for which both conditions are strictly fulfilled. Therefore, we conclude stating that the system (19) reverts to a system of two equations in two unknowns: the crack advancement Δ and the corresponding (minimum) failure load, represented either by the values K^*_{If} and K^*_{IIf} of the GSIFs in critical conditions or by the threshold value G_{0f} of G_0, implicitly embedded in the functions $\sigma_{\vartheta\vartheta}$ and $\mathcal{G}$. Exploiting

the well-known Irwin's relationship in plane strain and mixed mode:

$$\mathcal{G}(a) = \frac{K_{\mathrm{I}}^2(a)}{E'} + \frac{K_{\mathrm{II}}^2(a)}{E'} \tag{20}$$

the system (19) becomes:

$$\begin{cases} \int_0^{\Delta} \left[K_{\mathrm{I}}^2(a') + K_{\mathrm{II}}^2(a')\right] \mathrm{d}a' = K_{\mathrm{Ic}}^2 \Delta \\ \int_0^{\Delta} \sigma_{\vartheta\vartheta}(r) \mathrm{d}r = \sigma_{\mathrm{u}} \Delta \end{cases} \tag{21}$$

It is worth observing that the failure load estimate provided by the system (21) does depend on the crack propagation direction ϑ (see Fig. 1(b)). Among all the possible directions, the actual one will be the direction ϑ_{c} providing the minimum failure load.

Upon substitution of the SIFs Eq. (18) into the first equation of the system (21) and integrating between 0 and Δ, we get:

$$G_0^2 d_0^2 \left[\bar{\mu}_{11} \left(\frac{\Delta}{d_0}\right)^{2\lambda_{\mathrm{I}}} + \bar{\mu}_{12} \left(\frac{\Delta}{d_0}\right)^{\lambda_{\mathrm{I}}+\lambda_{\mathrm{II}}} + \bar{\mu}_{22} \left(\frac{\Delta}{d_0}\right)^{2\lambda_{\mathrm{II}}} \right] = K_{\mathrm{Ic}}^2 \Delta \tag{22}$$

where, for the sake of simplicity, we have introduced the angular functions:

$$\bar{\mu}_{11} = \frac{\mu_{11}^2 + \mu_{21}^2}{2\lambda_{\mathrm{I}}} \tag{23a}$$

$$\bar{\mu}_{12} = 2\frac{\mu_{11}\mu_{12} + \mu_{21}\mu_{22}}{\lambda_{\mathrm{I}} + \lambda_{\mathrm{II}}} \tag{23b}$$

$$\bar{\mu}_{22} = \frac{\mu_{12}^2 + \mu_{22}^2}{2\lambda_{\mathrm{II}}} \tag{23c}$$

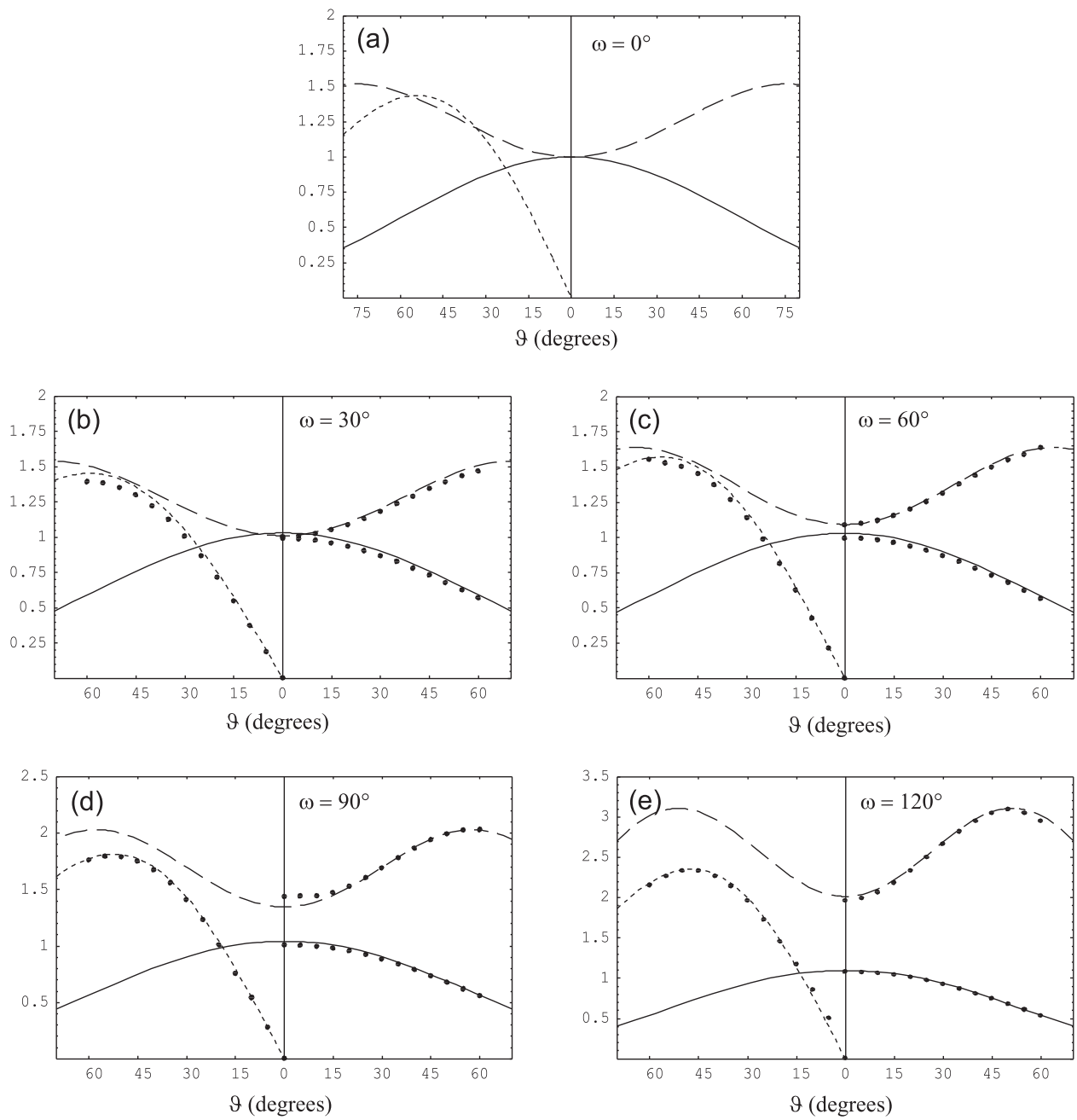

Fig. 4. Angular functions for the evaluation of the change in the strain energy for different notch opening angles ω: $\bar{\mu}_{11}$, continuous line; $\bar{\mu}_{12}$, dotted line; $\bar{\mu}_{22}$, dashed line. Plot (a) refers to $\omega = 0°$, (b) to $\omega = 30°$, (c) to $\omega = 60°$, (d) to $\omega = 90°$ and (e) to $\omega = 120°$. Black circles represent the numerical value provided in Yosibash et al. (2006). Note that $\bar{\mu}_{11}$ and $\bar{\mu}_{22}$ are symmetric, while $\bar{\mu}_{12}$ is anti-symmetric. For the sake of clarity, only the left half of the $\bar{\mu}_{12}$-function has been plotted.

An equivalent expression for Eq. (22) can be obtained substituting Eq. (11) into the first equation of the system (21), yielding:

$$\bar{\mu}_{11}\Delta^{2\lambda_I}\left(K_I^*\right)^2+\bar{\mu}_{12}\Delta^{\lambda_I+\lambda_{II}}K_I^*K_{II}^*+\bar{\mu}_{22}\Delta^{2\lambda_{II}}\left(K_{II}^*\right)^2=K_{Ic}^2\Delta \tag{24}$$

Eq. (24) highlights that the variation in the elastic energy is a quadratic function of the GSIFs. Eq. (24) can be found also in Yosibash et al. (2006), where it was derived in a different way, i.e. by directly computing coefficients $\bar{\mu}_{ij}$ of the quadratic form by suitable path independent integrals of the stress and displacement fields before and after the appearance of the finite crack advancement Δ. In Yosibash et al. (2006) the $\bar{\mu}_{ij}$ values can be found tabulated every 5 degrees in the range $0° < \vartheta < 60°$ and for notch opening angle ω equal to 30°, 60°, 90° and 120°. The comparisons between the values provided by Yosibash et al. (2006) and the ones derived here on the basis of the analysis by Beghini et al. (2007) are plotted in Fig. 4. A fairly good agreement is generally observed. The difference in the $\bar{\mu}_{11}$ values for $\vartheta = 0°$ is below 3% and the highly accurate data provided by Philipps et al. (2008) for the mode I case lie in between, so that it is hard to discriminate which values are more precise. In the following we keep on using the ones based on the analysis by Beghini et al. (2007) since, being expressed by interpolating functions, they allow a deeper analytical treatment of the problem under examination. Furthermore, they have a broader range of validity. The plots for $\omega = 0°$ (Fig. 4(a)) have been obtained by interpolating numerically the discrete values analytically computed by Melin (1994).

Upon substitution of the stress field represented by Eq. (5) into the second equation of the system (21) and integrating between 0 and Δ, we get:

$$G_0 d_0\left[\bar{f}^{I}_{\vartheta\vartheta}\left(\frac{\Delta}{d_0}\right)^{\lambda_I}+\bar{f}^{II}_{\vartheta\vartheta}\left(\frac{\Delta}{d_0}\right)^{\lambda_{II}}\right]=\sigma_u\Delta \tag{25}$$

where, for the sake of simplicity, we have introduced the angular functions:

$$\bar{f}^{I}_{\vartheta\vartheta}=\frac{f^{I}_{\vartheta\vartheta}}{\lambda_I(2\pi)^{1-\lambda_I}} \tag{26a}$$

$$\bar{f}^{II}_{\vartheta\vartheta}=\frac{f^{II}_{\vartheta\vartheta}}{\lambda_{II}(2\pi)^{1-\lambda_{II}}} \tag{26b}$$

An expression equivalent to Eq. (25) but expressed in terms of the GSIFs can be obtained substituting Eq. (1b) into the second equation of the system (21), yielding:

$$\bar{f}^{I}_{\vartheta\vartheta}\Delta^{\lambda_I}K_I^*+\bar{f}^{II}_{\vartheta\vartheta}\Delta^{\lambda_{II}}K_{II}^*=\sigma_u\Delta \tag{27}$$

5. Failure load in terms of the notch driving force G_0

Let us introduce the normalized mode mixity length δ_0 and the normalized crack advancement δ, defined as:

$$\delta_0=\frac{d_0}{l_{ch}}=\left(\frac{K_I^*}{K_{II}^*}\right)^{\frac{1}{\lambda_{II}-\lambda_I}}\left(\frac{\sigma_u}{K_{Ic}}\right)^2,\quad \delta=\frac{\Delta}{l_{ch}} \tag{28}$$

Note that, on the basis of the definition of the mode mixity ψ (Eq. (9)), the normalized mode mixity length δ_0 is also equal to:

$$\delta_0=(\tan\psi)^{-\frac{1}{\lambda_{II}-\lambda_I}} \tag{29}$$

Substitution of Eqs. (22) and (25) into the system (21) yields:

$$\begin{cases}\left(\frac{G_0}{\sigma_u}\right)^2=\dfrac{\delta/\delta_0^2}{\bar{\mu}_{11}\left(\frac{\delta}{\delta_0}\right)^{2\lambda_I}+\bar{\mu}_{12}\left(\frac{\delta}{\delta_0}\right)^{\lambda_I+\lambda_{II}}+\bar{\mu}_{22}\left(\frac{\delta}{\delta_0}\right)^{2\lambda_{II}}}\\ \frac{G_0}{\sigma_u}=\dfrac{\delta/\delta_0}{\bar{f}^{I}_{\vartheta\vartheta}\left(\frac{\delta}{\delta_0}\right)^{\lambda_I}+\bar{f}^{II}_{\vartheta\vartheta}\left(\frac{\delta}{\delta_0}\right)^{\lambda_{II}}}\end{cases} \tag{30}$$

which can be rewritten equivalently as:

$$\begin{cases}\frac{G_0}{\sigma_u}=\dfrac{\delta/\delta_0}{\bar{f}^{I}_{\vartheta\vartheta}\left(\frac{\delta}{\delta_0}\right)^{\lambda_I}+\bar{f}^{II}_{\vartheta\vartheta}\left(\frac{\delta}{\delta_0}\right)^{\lambda_{II}}}\\ \delta-\dfrac{\left[\bar{f}^{I}_{\vartheta\vartheta}\left(\frac{\delta}{\delta_0}\right)^{\lambda_I}+\bar{f}^{II}_{\vartheta\vartheta}\left(\frac{\delta}{\delta_0}\right)^{\lambda_{II}}\right]^2}{\bar{\mu}_{11}\left(\frac{\delta}{\delta_0}\right)^{2\lambda_I}+\bar{\mu}_{12}\left(\frac{\delta}{\delta_0}\right)^{\lambda_I+\lambda_{II}}+\bar{\mu}_{22}\left(\frac{\delta}{\delta_0}\right)^{2\lambda_{II}}}=0\end{cases} \tag{31}$$

The second equation presents a unique unknown, the dimensionless crack advancement δ, but it cannot be solved analytically. However, in this form the determination of the failure load appears as a standard minimization problem under constraint. In fact, for a given geometry, loading configuration and material, ω and δ_0 are fixed: according to the first equation of the system (31), the critical load depends only on the dimensionless crack advancement δ and on the crack initiation angle ϑ through the angular functions. Hence we can re-write formally the system (31) as:

$$\begin{cases}\dfrac{G_0}{\sigma_u}=A_1(\delta,\vartheta)\\ A_2(\delta,\vartheta)=0\end{cases} \tag{32}$$

It is thus clear that we are seeking the values δ_c and ϑ_c which minimize the (dimensionless) failure load A_1 under the constraint $A_2 = 0$. According to the mathematical technique of Lagrange multipliers, the determination of the minimum of a function of n variables (in the present case $n = 2$) under a constraint can be recast into the problem of finding the stationary point of a function F of $n + 1$ variables, represented in this case by:

$$F(\delta,\vartheta,\lambda)=A_1(\delta,\vartheta)+\lambda A_2(\delta,\vartheta) \tag{33}$$

where λ is the so-called Lagrange multiplier, which should not be confused with the eigenvalues λ_I and λ_{II}. The stationary point is found by setting to zero the partial first derivatives of function F:

$$\begin{cases}\dfrac{\partial F}{\partial\delta}=0\\ \dfrac{\partial F}{\partial\vartheta}=0\\ \dfrac{\partial F}{\partial\lambda}=0\end{cases} \tag{34}$$

Although rather complicated, the expressions of the first partial derivatives of function F can be obtained analytically. Finally, the numerical solution of system (34) is readily achieved, with any desired accuracy, by starting from a trial point and proceeding towards the solution with Newton's method. We have had no numerical problems in seeking the solution except in loading case very close to pure mode I and pure mode II; however these particular cases will be dealt with specifically later.

The solution of the system (34) provides, beyond the value of the Lagrange multiplier (which is a dummy variable), the actual crack advancement δ_c and crack initiation angle ϑ_c. Substituting these values in the first equation of system (31) yields finally the value of the notch driving force at incipient failure G_{0f}, which is proportional to the failure load. The values of the crack orientation and of the normalized critical notch driving force are given in Tables 2 and 3 and plotted in Figs. 5 and 6. Since δ_0 can vary between 0 (pure mode II) and infinity (pure mode I), we prefer to plot the load and the crack orientation vs. the mode mixity angle ψ instead of the dimensionless mixity length δ_0, since ψ is limited between 0 (pure mode I) and $\pi/2$ (pure mode II); ψ and δ_0 are related by the one-to-one relationship given by Eq. (29).

The lengths of the dimensionless finite crack advancements δ_c represent a secondary result of the present approach and therefore are not tabulated. Nevertheless it is worth observing that δ_c shows a modest overall variation, its highest value being $2/\pi$ (i.e. $\Delta_c \cong 0.637\, l_{ch}$) for a crack under mode I loading and slightly decreasing for larger notch opening angles and mode mixities.

Table 2
Crack deflection with respect to the notch bisector for different re-entrant corner amplitudes (ω) and mode mixities (ψ). The last column represents the crack deflection ϑ_{IIc} in pure mode II and is reported for the sake of clarity also in Table 1.

$\lvert\vartheta_c\rvert$ [°]		ψ [°]									
		0	10	20	30	40	50	60	70	80	90
ω [°]	0	0	19.1	34.4	45.4	53.4	59.4	64.3	68.4	72.2	75.6
	20	0	20.4	35.1	45.1	52.2	57.5	61.6	65.2	68.3	71.2
	30	0	20.4	34.9	44.5	51.0	55.8	59.6	62.8	65.6	68.2
	40	0	20.6	34.6	43.5	49.6	54.1	57.6	60.6	63.2	65.7
	50	0	20.9	34.2	42.5	48.2	52.3	55.6	58.4	60.9	63.3
	60	0	21.0	33.7	41.5	46.7	50.5	53.6	56.2	58.5	60.9
	70	0	21.1	33.1	40.4	45.2	48.7	51.6	54.0	56.3	58.5
	80	0	21.0	32.5	39.2	43.7	47.0	49.6	52.0	54.1	56.3
	90	0	20.8	31.7	38.0	42.1	45.2	47.7	49.9	51.9	54.0
	100	0	20.6	30.9	36.7	40.6	43.4	45.7	47.8	49.8	51.8

Table 3
Ratio of the value of the notch driving force at incipient failure (G_{0f}) to the material tensile strength (σ_u) for different re-entrant corner amplitudes (ω) and mode mixities (ψ).

G_{0f}/σ_u		ψ [°]									
		0	10	20	30	40	50	60	70	80	90
ω [°]	0	–	–	–	–	–	–	–	–	–	–
	20	–	7.23E−7	2.31E−4	8.36E−3	1.45E−1	2.02	3.21E+1	9.39E+2	1.77E+5	–
	30	-	1.23E−4	4.60E−3	4.26E−2	2.45E−1	1.21	6.41	4.79E+1	1.06E+3	–
	40	–	1.57E−3	2.03E−2	9.55E−2	3.18E−1	9.43E−1	2.89	1.10E+1	8.47E+1	–
	50	–	7.16E−3	4.90E−2	1.55E−1	3.72E−1	8.13E−1	1.80	4.60	1.88E+1	–
	60	–	1.97E−2	8.82E−2	2.13E−1	4.12E−1	7.36E−1	1.31	2.58	6.92	–
	70	–	4.05E−2	1.34E−1	2.67E−1	4.43E−1	6.85E−1	1.05	1.70	3.38	–
	80	–	7.00E−2	1.84E−1	3.17E−1	4.68E−1	6.47E−1	8.81E−1	1.23	1.96	–
	90	–	1.08E−1	2.37E−1	3.62E−1	4.86E−1	6.16E−1	7.64E−1	9.54E−1	1.27	–
	100	–	1.54E−1	2.90E−1	4.03E−1	5.00E−1	5.89E−1	6.76E−1	7.68E−1	8.78E−1	–

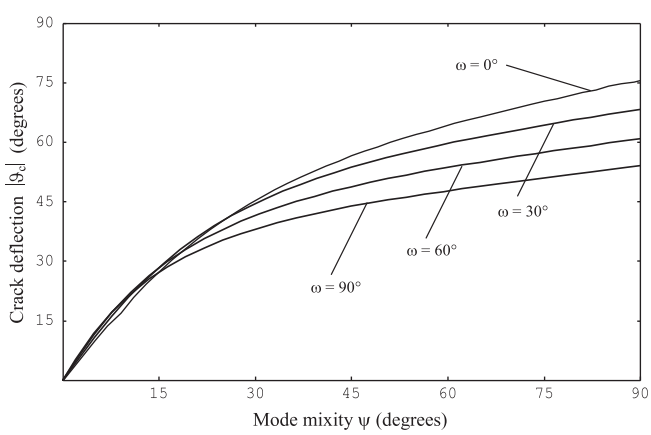

Fig. 5. Crack deflection vs. mode mixity for different notch opening angle.

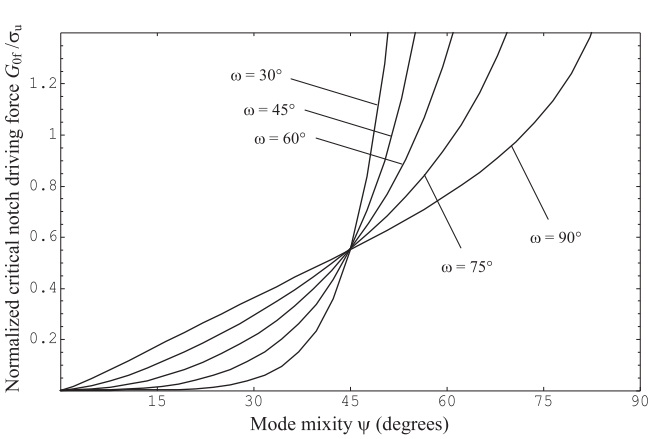

Fig. 6. Critical notch driving force vs. mode mixity for different notch opening angles.

The present analytical treatment is very useful for the subsequent parametric analysis. The alternative procedure (exploited in Yosibash et al. (2006)) is to compute (for each ω and ψ pair) the failure load for different ϑ values: the actual crack propagation angle ϑ_c is the one providing the minimum failure load. It is evident that this latter procedure is trickier and limited to a discrete set of ϑ values (every 5° in Yosibash et al. (2006)), while the present analysis does not introduce further numerical errors beyond the approximation embedded in the weight functions (14).

Summarizing, the determination of the failure load of a V-notched homogeneous structure made of a material with tensile strength σ_u and fracture toughness K_{Ic} can be achieved by means of the following steps:

(1) Determine K_I^* and K_{II}^*, i.e. the shape functions defining the proportionality between the GSIFs and the applied load by means of a linear elastic Finite Element Analysis (FEA) and a suitable technique, e.g. the H-integrals (Sinclair et al., 1984).
(2) Compute the mode mixity ψ through Eq. (9).
(3) Determine the value of the direction of crack propagation ϑ_c and of the notch driving force at failure G_{0f} from Tables 2 and 3 or from Figs. 5 and 6.
(4) Compute the failure load by equating the notch driving force (Eq. (3)) with its critical value G_{0f} by means of the proportionality factors between the GSIFs and the applied load (point 1).

Although several papers have dealt with the analysis of V-notched structures under mixed mode loading, we believe that universal diagrams such as the ones in Figs. 5 and 6 are original, and not only for the fracture propagation criterion chosen (FFM in the present case). In fact, plots or tables available in the literature usually provide the failure load (thus including the shape functions) vs. the (dimensional) ratio between the GSIFs (e.g. Yos-

ibash et al., 2006) or vs. the (dimensionless) ratio between the shear and normal force over the whole ligament (Seweryn and Lukaszewicz, 2002). Since both the ratios do not define univocally the mode mixity ψ, unless l_{ch} is fixed, these plots are limited to a specific geometry and material, a shortcoming that diagrams in Figs. 5 and 6 do not show.

For what concerns Fig. 5, it shows how the crack orientation ϑ_c varies along with the mode mixity ψ for different notch opening angles ω. Note that for positive K^*_{II} (and, therefore, for positive ψ), according to the chosen polar reference system (Fig. 1(b)), the crack orientation of the V-notch emanated crack is negative and vice versa; since the ϑ_c vs. ψ diagram is antisymmetric, for the sake of clarity, in Fig. 5 we plotted the absolute value $|\vartheta_c|$ only for positive ψ value. As expected, the crack deflection increases along with the mode mixity, being zero in mode I and reaching a maximum in mode II. Note that the slope of the curves is higher for low mode mixity and smaller for higher mode mixity. A second trend is that increasing the notch opening angle ω, the crack deflection (with respect to the notch bisector) is generally smaller, i.e. higher deflections tend to occur in the crack case. Further comments about the mode II crack deflection will be provided later.

About Fig. 6, it is observed that the critical value G_{0f} of the notch driving force increases monotonically with the mode mixity (note this trend does not imply that the failure load increases, since it depends also on the shape functions), showing almost the same value for $\psi = 45°$. It is also evident that G_{0f} shows strong numerical variations for different ω and ψ values, so that the notch driving force G_0 is awkward to determine graphically the failure load. This fact, together with the impossibility to use the G_0 description for pure mode I, for pure mode II (for such extreme cases, in fact, G_{0f} is either zero or infinite, respectively, for any ω) and for the crack case, suggests us to provide the failure load also in a more traditional form, i.e. highlighting the safety domain in terms of the GSIFs. This task will be the subject of the following section.

6. Failure load in terms of the GSIFs K^*_I and K^*_{II}

We start revisiting the results for pure mode I obtained in Carpinteri et al. (2008). They will be used later for a proper normalization of the safety region in case of mixed mode loading.

6.1. Pure mode I

Under pure mode I loading condition, for symmetry reason the crack propagates along the notch bisector, i.e. $\vartheta_c = \vartheta_{Ic} = 0$. As observed in the previous section, the description in terms of (G_0,d_0) is not possible. Hence, we are forced to use the GSIF. Upon substitution of Eqs. (24) and (27), limited to the mode I contributions, into the system (21), we get:

$$\begin{cases} \bar{\mu}_{11}\Delta^{2\lambda_I}\left(K^*_I\right)^2 = K^2_{Ic}\Delta \\ \bar{f}^{I}_{\vartheta\vartheta}\Delta^{\lambda_I}K^*_I = \sigma_u\Delta \end{cases} \tag{35}$$

The system (35) is readily solved, yielding the crack advancement Δ_c and the critical value K^*_{Ic} of the mode I GSIF K^*_I under pure mode I loading, i.e. the generalized fracture toughness:

$$K^*_{Ic} = \xi(\omega)K^{2(1-\lambda_I)}_{Ic}\sigma^{2\lambda_I-1}_u = \xi(\omega)\sigma_u l^{1-\lambda_I}_{ch} \tag{36}$$

where:

$$\xi(\omega) = \lambda_I^{\lambda_I}\left[\frac{2(2\pi)^{2\lambda_I-1}}{\mu^2_{11}(\vartheta=0,\omega)}\right]^{1-\lambda_I} \tag{37}$$

Eq. (36) was derived in Carpinteri et al. (2008). Note that, since ξ is equal to unity for ω equal to 0 or π, the generalized fracture toughness equals the fracture toughness for a cracked geometry and the tensile strength for a flat edge. The ξ values for different notch opening angles ω are given in Table 1.

6.2. Mixed mode

In the case of mixed mode loading, the critical values of the GSIFs can be obtained either upon substitution of the critical value of the notch driving force G_{0f} into Eq. (4), or, directly, by substituting Eqs. (24) and (27) into the system (21). In the former way and normalizing the GSIFs with respect to the generalized fracture toughness K^*_{Ic} and to Irwin's length l_{ch}, we get:

$$\frac{K^*_{If}}{K^*_{Ic}} = \frac{(\tan\psi)^{-\frac{1-\lambda_I}{\lambda_{II}-\lambda_I}}}{\xi}\frac{G_{0f}}{\sigma_u} \tag{38a}$$

$$\frac{K^*_{IIf}}{l^{\lambda_I-\lambda_{II}}_{ch}K^*_{Ic}} = \frac{(\tan\psi)^{-\frac{1-\lambda_{II}}{\lambda_{II}-\lambda_I}}}{\xi}\frac{G_{0f}}{\sigma_u} \tag{38b}$$

For the sake of completeness and for the subsequent analysis, it is interesting to proceed also directly. Thus the system (21) becomes:

$$\begin{cases} \left(\dfrac{K^*_I}{K^*_{Ic}}\right)^2 = \dfrac{\delta}{\xi^2(\bar{\mu}_{11}\delta^{2\lambda_I} + \bar{\mu}_{12}\delta^{\lambda_I+\lambda_{II}}\tan\psi + \bar{\mu}_{22}\delta^{2\lambda_{II}}\tan^2\psi)} \\ \dfrac{K^*_I}{K^*_{Ic}} = \dfrac{\delta}{\xi(\bar{f}^{I}_{\vartheta\vartheta}\delta^{\lambda_I} + \bar{f}^{II}_{\vartheta\vartheta}\delta^{\lambda_{II}}\tan\psi)} \end{cases} \tag{39}$$

where, recalling Eq. (9):

$$\tan\psi = \frac{K^*_{II}l^{\lambda_{II}-\lambda_I}_{ch}}{K^*_I} \tag{40}$$

The system (39) can be recast as:

$$\begin{cases} \dfrac{K^*_I}{K^*_{Ic}} = \dfrac{\delta}{\xi(\bar{f}^{I}_{\vartheta\vartheta}\delta^{\lambda_I} + \bar{f}^{II}_{\vartheta\vartheta}\delta^{\lambda_{II}}\tan\psi)} \\ \delta - \dfrac{\left(\bar{f}^{I}_{\vartheta\vartheta}\delta^{\lambda_I} + \bar{f}^{II}_{\vartheta\vartheta}\delta^{\lambda_{II}}\tan\psi\right)^2}{\bar{\mu}_{11}\delta^{2\lambda_I} + \bar{\mu}_{12}\delta^{\lambda_I+\lambda_{II}}\tan\psi + \bar{\mu}_{22}\delta^{2\lambda_{II}}\tan^2\psi} = 0 \end{cases} \tag{41}$$

The technique of Lagrange multipliers used to solve Eq. (31) can now be exploited to solve Eq. (41). In fact, Eq. (41) can be interpreted as a constrained minimization problem, since, once the geometry, material and loading are fixed (i.e. ω and ψ are given), the actual crack advancement δ_c and crack orientation ϑ_c are the ones that minimize the first equation, i.e. the dimensionless failure load K^*_{If} / K^*_{Ic}, under the constraint represented by the second equation. Once the critical value K^*_{If} of the mode I GSIF is determined, the corresponding critical value K^*_{IIf} of the mode II GSIF is provided by Eq. (40). The values K^*_{If}, K^*_{IIf} of the GSIFs at incipient failure are given in Tables 4 and 5 for different ω and ψ values.

Obviously, the values of the crack orientation angle coincide with the ones provided with the G_0 formalism, plotted in Fig. 5 and tabulated in Table 2. On the other hand, the critical values of the GSIFs can be plotted in the (K^*_I, K^*_{II}) plane for a given notch opening angle ω and varying the mode mixity ψ. In this way we obtain a curve delimiting a safety region, i.e. points lying in this domain correspond to admissible stress states, whereas points lying outside correspond to failure. It is convenient to plot the results in a dimensionless form: the mode I GSIF is normalized with respect to the generalized fracture toughness $K^*_{Ic} = \xi\sigma_u l^{1-\lambda_I}_{ch}$, whereas the mode II GSIF is normalized with respect to $K^*_{Ic}l^{\lambda_I-\lambda_{II}}_{ch} = \xi\sigma_u l^{1-\lambda_{II}}_{ch}$. The safety domain is plotted in Fig. 7, taking e.g. $\omega = 90°$. If the external loads are increased proportionally, the ratio between the GSIFs keeps constant. It means that in the (K^*_I, K^*_{II}) plane, the loading curve is represented by a straight line starting from the origin. Furthermore, in the dimensionless plane of Fig. 7, the angle between the loading path and the horizontal axis is exactly ψ, since the slope of the loading line is given by the right hand side of Eq. (40). According to the brittleness assumption, failure is attained suddenly when the straight line crosses the curve delimiting the safety domain, point A.

Table 4
Ratio of the value of mode I GSIF at incipient failure (K^*_{If}) to generalized fracture toughness (K^*_{Ic}) for different re-entrant corner amplitudes (ω) and mode mixities (ψ).

K^*_{If}/K^*_{Ic}		ψ [°]									
		0	10	20	30	40	50	60	70	80	90
ω [°]	0	1	0.957	0.854	0.731	0.608	0.488	0.372	0.255	0.133	0
	20	1	0.955	0.852	0.731	0.610	0.493	0.379	0.262	0.138	0
	30	1	0.955	0.852	0.733	0.614	0.498	0.383	0.266	0.141	0
	40	1	0.955	0.852	0.733	0.615	0.501	0.387	0.269	0.143	0
	50	1	0.953	0.850	0.733	0.616	0.502	0.389	0.271	0.145	0
	60	1	0.952	0.848	0.731	0.615	0.502	0.390	0.273	0.146	0
	70	1	0.950	0.845	0.728	0.613	0.501	0.389	0.273	0.146	0
	80	1	0.948	0.841	0.725	0.610	0.498	0.387	0.272	0.145	0
	90	1	0.946	0.837	0.719	0.604	0.494	0.384	0.269	0.144	0
	100	1	0.943	0.831	0.712	0.598	0.487	0.378	0.265	0.142	0

Table 5
Mode II GSIF at incipient failure (K^*_{IIf}) normalized with respect to $l_{ch}^{\lambda_I-\lambda_{II}} \times K^*_{Ic}$ for different re-entrant corner amplitudes (ω) and mode mixities (ψ). The last column represents the ratio $\eta = K^*_{IIc}/\left(l_{ch}^{\lambda_I-\lambda_{II}} \times K^*_{Ic}\right)$ and is reported for the sake of clarity also in Table 1.

$\frac{K^*_{IIf}}{l_{ch}^{\lambda_I-\lambda_{II}} K^*_{Ic}}$		ψ [°]									
		0	10	20	30	40	50	60	70	80	90
ω [°]	0	0	0.169	0.311	0.422	0.510	0.582	0.644	0.701	0.756	0.811
	20	0	0.168	0.310	0.422	0.512	0.588	0.656	0.719	0.783	0.849
	30	0	0.168	0.310	0.423	0.515	0.593	0.664	0.731	0.798	0.870
	40	0	0.168	0.310	0.423	0.516	0.597	0.670	0.740	0.811	0.887
	50	0	0.168	0.309	0.423	0.517	0.599	0.673	0.746	0.820	0.901
	60	0	0.168	0.309	0.422	0.516	0.599	0.675	0.749	0.826	0.910
	70	0	0.168	0.308	0.421	0.515	0.597	0.674	0.749	0.827	0.913
	80	0	0.167	0.306	0.418	0.512	0.594	0.671	0.746	0.825	0.912
	90	0	0.167	0.305	0.415	0.507	0.589	0.664	0.739	0.817	0.904
	100	0	0.166	0.302	0.411	0.501	0.581	0.655	0.728	0.804	0.890

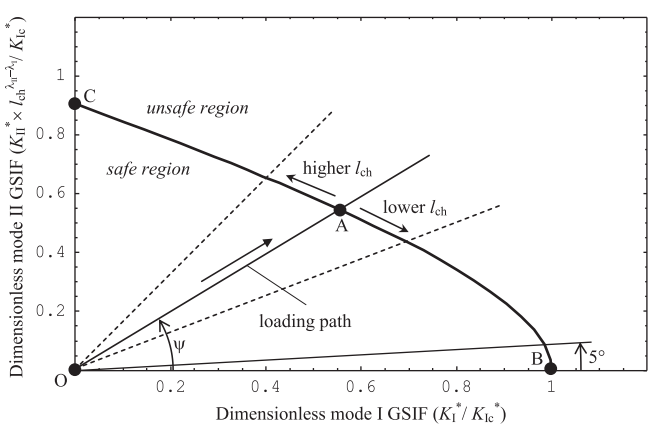

Fig. 7. Resistance domain in the GSIFs plane ($\omega = 90°$): points lying beneath the thick curve correspond to admissible stress states and vice versa. For mode mixities ψ lower than 5°, the mode II effect on the critical load can be neglected from an engineering point of view.

Apart from substitution of the SIFs with the GSIFs, this behavior strictly resembles what occurs in the classical crack branching problem. Indeed, as we will show later, the crack branching problem is a particular case of the present one, taking place for $\omega = 0°$. However there is a substantial difference with respect to the crack kinking problem: if $\omega > 0°$, the mode mixity ψ depends also on the material brittleness through l_{ch} (see Eq. (40)) and not only on the loading, i.e. on the GSIFs ratio. For a given K^*_{II}/K^*_I ratio, the slope of the loading line will diminish for brittle materials (low l_{ch}), while will increase for less brittle materials (high l_{ch}): in other words, whatever is the GSIF ratio, the failure point migrates towards point B (pure mode I failure) as material brittleness increases, whereas it moves towards point C, if the brittleness decreases (within a certain range, otherwise, as explained in the following section, the asymptotic approach does not hold any more).

As clearly shown by Eq. (9) or (40), the effect of the material on the mode mixity increases as the notch opening increase. In fact, for larger ω, the gap between the Williams eigenvalues λ_{II} and λ_I grows. On the other hand, for a vanishing notch opening angle, both λ_{II} and λ_I tend to 1/2 and the effect of the material vanishes. This material dependence is valid also for the orientation of the V-notch emanated crack, see Fig. 5: as brittleness increases, l_{ch} diminishes, ψ diminishes and the crack deflection ϑ_c tends to zero, i.e. the V-notch emanated crack tends to propagate in mode I along the bisector. On the other hand, for less brittle material, the crack deflection is higher under the same GSIFs ratio. Once more, it is worth emphasizing the fundamental difference with respect to the crack case, where the angle of the crack kinking depends only on the (dimensionless) SIFs ratio, i.e. is the same independently of the material.

In Fig. 8 we plotted the safety domains for different notch opening angles ω. It is evident that all the curves are similar. Of course, this fact does not imply that the failure load does not vary with ω, since the physical dimensions as well as the shape functions defining the GSIFs vary along with ω. It simply shows that the transition from mode I to mode II fracture is approximately the same for all the notch amplitudes. Moreover, the shape of these curves, showing a vertical tangent at the intercept with the horizontal axis, suggests defining a threshold value of the mode mixity angle below which failure can be considered as occurring in pure mode I. We can assume, for instance, a threshold value equal to 5° (see Fig. 7). In fact, if $\psi < 5°$, neglecting the effect of the mode II component (i.e. assuming that failure occurs when $K^*_I = K^*_{Ic}$, point B in Fig. 7) means to overestimate the failure load of no more than 2% (for any ω value), an accuracy which is considered acceptable for engineering purposes. Note that, while the mode II component can be neglected for what concerns the failure load provided

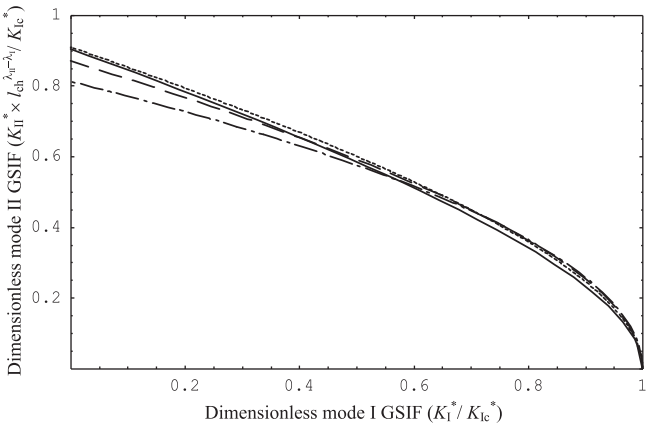

Fig. 8. Safety domains in the GSIFs plane for different notch opening angles: continuous line, $\omega = 90°$; dotted line, $\omega = 60°$; dashed line, $\omega = 30°$; dot-dashed line, $\omega = 0°$.

$\psi < 5°$, it is not negligible as regards the crack deflection, since, even a small mode II contribution causes a significant deflection of crack propagation from the notch bisector (see Fig. 5).

6.3. Pure mode II

The material does not affect the mode mixity ψ for $\omega = 0°$ (cracked geometries) and, whatever is the notch amplitude, for pure mode I and mode II loadings, when the mode mixity is equal to 0° and 90°, respectively (see Eq. (40)). Pure mode I loadings have been already dealt with. For what concerns pure mode II, we can replace K_I^* with K_{II}^* by means of Eq. (40) in the system (39). Then, letting $\psi \to \pi/2$, we get:

$$\begin{cases} \left(\dfrac{K_{II}^*}{l_{ch}^{\lambda_I-\lambda_{II}} K_{Ic}^*}\right)^2 = \dfrac{\delta^{1-2\lambda_{II}}}{\xi^2 \bar{\mu}_{22}} \\ \dfrac{K_{II}^*}{l_{ch}^{\lambda_I-\lambda_{II}} K_{Ic}^*} = \dfrac{\delta^{1-\lambda_{II}}}{\xi \bar{f}_{\vartheta\vartheta}^{II}} \end{cases} \tag{42}$$

Differently from the general mixed mode case, for pure mode II we can get an analytical solution for the dimensionless crack advancement by taking the square of the second equation and equating. Substitution in the first or the second equation provides:

$$\frac{K_{II}^*}{l_{ch}^{\lambda_I-\lambda_{II}} K_{Ic}^*} = \frac{1}{\xi (\bar{f}_{\vartheta\vartheta}^{II})^{2\lambda_{II}-1} (\bar{\mu}_{22})^{1-2\lambda_{II}}} \tag{43}$$

The mode II GSIF given by Eq. (43) depends on the crack propagation angle ϑ: the actual value, i.e. ϑ_{IIc}, will be the one providing the minimum mode II GSIF value, i.e. K_{IIc}^*. Equivalently, the crack propagation angle is the one maximizing the denominator at the right hand side in Eq. (43). This value can be easily achieved by setting to zero its derivative:

$$\frac{d}{d\vartheta}\left[(\bar{f}_{\vartheta\vartheta}^{II})^{2\lambda_{II}-1} (\bar{\mu}_{22})^{1-2\lambda_{II}}\right] = 0 \tag{44}$$

Thanks to the analytical expressions of the angular functions Eqs. (23) and (26), the derivative (44) can be calculated explicitly and solved numerically with the desired accuracy. We mark with $\vartheta_{IIc}(\omega)$ its solution, and with $\eta(\omega)$ the corresponding (minimum) value of the right hand side of Eq. (43), so that the critical value K_{IIc}^* of the mode II GSIF under pure mode II loading is:

$$K_{IIc}^* = \eta(\omega) l_{ch}^{\lambda_I-\lambda_{II}} K_{Ic}^* = \eta(\omega)\xi(\omega)\sigma_u l_{ch}^{1-\lambda_{II}} \tag{45}$$

Numerical values for ϑ_{IIc} and η are reported in Table 1 for different values of the re-entrant corner amplitude ω. While η shows a modest variation, its values being comprised between 0.8 and 1, the crack deflection ϑ_{IIc} shows significant changes. As evident from Fig. 9, ϑ_{IIc} decreases (in modulus) as the notch amplitude increases: more in details, it decreases almost linearly from 75.6° for $\omega = 0°$ (i.e. for a crack) to 51.3° for $\omega = 102.6°$, when the mode II singularity disappears. Values of η and ϑ_{IIc} computed here have been used for the plots in Fig. 5 (point at the right extreme), in Fig. 7 (point C) and Fig. 8 (intercepts with the vertical axis).

6.4. Cracked geometries

For cracked geometries, the notch opening angle vanishes, i.e. $\omega = 0°$. Accordingly, both the modes show the same 0.5 singularity, being $\lambda_I = \lambda_{II} = 1/2$, and the GSIFs reverts to the classical SIFs. Moreover ξ (Eq. (37)) is equal to unity.

It is easy to show that, for cracks, FFM reverts to the classical Griffith criterion, i.e. fracture occurs in the direction where the strain energy release rate is maximum and reaches its critical value, the fracture energy. In fact, if we consider the energy balance, i.e. Eq. (24), the crack advancements at left and right hand side cancel each other out. It means that the failure load is given only by the energy equation: the stress requirement contributes only in the determination of the crack advancement. In other words, the discrete energy balance, being independent of the crack advancement, coincides with Griffith's condition for the crack to propagate:

$$\mathcal{G} = \frac{\overline{K}_I^2 + \overline{K}_{II}^2}{E'} = \mathcal{G}_c \tag{46}$$

Eq. (46) represents the well-known $\mathcal{G}$-max criterion for the kinked crack problem (see, e.g., Wu, 1978; Hayashi and Nemat-Nasser, 1981). For the sake of completeness and comparison with the V-notched emanated crack problem, here we recall its basic features.

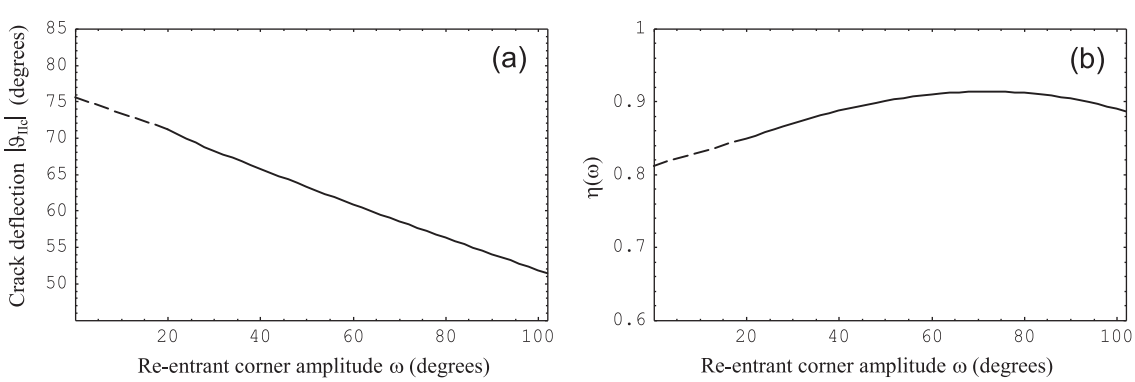

Fig. 9. Orientation of the V-notch emanated crack (a) and dimensionless generalized fracture toughness (b) for pure mode II loading configurations vs. notch opening angle ω. Values for $0° < \omega < 20°$ (dashed part of the curves) are linearly interpolated between the cracked ($\omega = 0°$) and the notched (with $20° \leqslant \omega \leq 102.6°$) geometries.

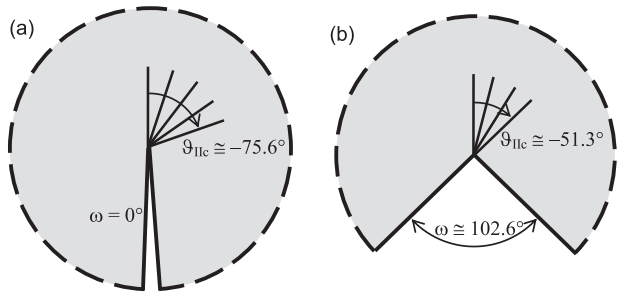

Fig. 10. Admissible crack deflections ϑ_c for cracked ($\omega = 0°$, (a)) and $\omega \cong 102.6°$ (limit value for which both modes are singular, (b)) geometries. The crack deflection increases with the mode mixity ψ and (generally) decreases with increasing re-entrant corner amplitude ω. Note that for $\omega \cong 102.6°$ and pure mode II loading, the V-notch emanated crack propagates along the notch flank direction.

The value of the SIFs $\overline{K}_I, \overline{K}_{II}$ of the kinked crack (see Fig. 1(c)) can be expressed as a function of the SIFs K_I,K_{II} of the main crack by means of Eq. (13). The values of the coefficients μ_{ij} vs. ϑ can be obtained by a suitable interpolation of the discrete value provided in Melin (1994). Upon substitution of Eq. (13) into Eq. (46), we finally get:

$$\left(\frac{K_I}{K_{Ic}}\right)^2 = \frac{1}{\bar{\mu}_{11} + \bar{\mu}_{12}\tan\psi + \bar{\mu}_{22}\tan^2\psi} \tag{47}$$

which, obviously, coincides with the first equation of the FFM system (39), provided that $\lambda_I = \lambda_{II} = 1/2$. It is worth emphasizing that now the mode mixity, Eq. (40), simplifies into:

$$\tan\psi = \frac{K_{II}}{K_I} \tag{48}$$

and, therefore, the mode mixity does not depend on the material, but only on the (dimensionless) ratio of the SIFs. The crack propagation angle ϑ_c is the one minimizing the failure load, i.e. the mode I SIF in Eq. (47). The values obtained have been exploited to plot the $\omega = 0°$ curves in Figs. 5 and 8. In case of pure mode II, by Eq. (48) we can replace K_I with K_{II} in Eq. (47) so that, letting $\psi \to \pi/2$, we get:

$$\left(\frac{K_{II}}{K_{Ic}}\right)^2 = \frac{1}{\bar{\mu}_{22}} \tag{49}$$

As evident from Fig. 4a, the crack deflection minimizing the mode II SIF is $\vartheta_{IIc} = -75.6°$ (see Fig. 10(a)) while the ratio $\eta = K_{IIc}/K_{Ic}$ (see Eq. (45)) is equal to 0.811. These values were used to plot the initial values in the two plots of Fig. 9.

6.5. Non-singular stress field

The lowest re-entrant corner amplitude for which the stress field is no more singular is $\omega \cong 102.6°$, when the notch is solicited in pure mode II. This case can be considered dual to the previous one, since FFM reverts to the classical strength criterion, i.e. fracture occurs in the direction where the circumferential stress is maximum and reaches its critical value, the tensile strength. In fact, being $\lambda_{II} = 1$, Eq. (1b) becomes:

$$\sigma_{\vartheta\vartheta}(\vartheta) = K^*_{II} f^{II}_{\vartheta\vartheta}(\vartheta) \tag{50}$$

i.e. the stress field is constant with respect to the radial coordinate, while being still dependent on the angular one. It is worth observing that the mode II GSIF K^*_{II} acquires the physical dimensions of a stress. More precisely, K^*_{II} coincides with the shearing stress τ along the notch bisector, since, being $f^{II}_{r\vartheta}(\vartheta = 0) = 1$ (see Appendix A), Eq. (1c) becomes:

$$\tau_{r\vartheta}(\vartheta = 0) = K^*_{II} = \tau \tag{51}$$

Since the stress field is constant with respect to r, the average stress condition for crack propagation turns to be independent of the crack advancement. It means that the failure load is given only by the stress condition: the energy balance contributes only in the determination of the crack advancement. In fact, substitution of Eq. (50) into second equation of the system (21) directly yields:

$$\frac{\tau}{\sigma_u} = \frac{1}{f^{II}_{\vartheta\vartheta}(\vartheta)} \tag{52}$$

which can be further regarded as a particular case ($\lambda_{II} = 1$) of the second equation in Eq. (42). The actual crack deflection ϑ_{IIc} is the one minimizing the failure load, i.e. the shearing stress τ in Eq. (52), or, equivalently, ϑ_{IIc} is the value maximizing $f^{II}_{\vartheta\vartheta}$. Recalling that:

$$\frac{df^{I}_{\vartheta\vartheta}(\vartheta)}{d\vartheta} = -(1 + \lambda_I) f^{I}_{r\vartheta}(\vartheta) \tag{53a}$$

$$\frac{df^{II}_{\vartheta\vartheta}(\vartheta)}{d\vartheta} = -(1 + \lambda_{II}) f^{II}_{r\vartheta}(\vartheta) \tag{53b}$$

ϑ_{IIc} is also the solution of the following equation:

$$f^{II}_{r\vartheta}(\vartheta) = 0 \tag{54}$$

implying that, in this very particular case, crack propagates in the direction where the shear stress vanishes. By means of Eq. (A.8) with $\lambda_{II} = 1$, Eq. (54) becomes:

$$\frac{\cos(2\vartheta) - \cos\omega}{1 - \cos\omega} = 0 \tag{55}$$

where the root $\vartheta_{IIc} = -\omega/2$ is the one corresponding to the minimum (dimensionless) failure load $\tau_c/\sigma_u = 0.892$ (divided by ξ this value provides the ordinate of the final point of the plot in Fig. 9(b)). Eq. (55) shows that, for $\omega \cong 102.6°$ and under pure mode II loading, the V-notch emanated crack grows along the notch flank direction (Fig. 10(b)).

One can wonder what happens for re-entrant corner larger than 102.6°. From a physical point of view, no strong differences are expected, although it can be easily argued that mode I will be even more dominant since the difference between the eigenvalues λ_{II} and λ_I further increases as $\omega \to 180°$. However, the asymptotic approach fails in providing a reliable estimate of the failure load, at least partially. In fact, if $\omega > 102.6°$, then $\lambda_{II} > 1$, implying that the mode II component of the stress field (Eq. (1)) is monotonically increasing with the distance from the notch tip. The search for the global minimum will thus lead to a vanishing failure load and infinite crack advancement. This meaningless result is obviously due to the indefinitely increasing stress field, which is a shortcoming of the asymptotic approach without a physical background. Maybe local minima, corresponding to real critical condition, could occur. Further research in this direction is still needed.

7. Average stress criterion

In this section we provide the solution in terms of V-notch emanated crack deflection and critical values of the GSIFs for the average stress criterion. This criterion, dating back to Novozhilov (1969) and applied to V-notch since Seweryn (1994), lacks a clear physical background because it is not based on an energy balance which, since the pioneering work of Griffith, represents the essence of Fracture Mechanics. Nevertheless, it usually provides failure load estimates close to the ones given by more refined models. This observation, together with its simplicity, is the cause of its wide spreading in engineering analyses (e.g. Taylor, 2007).

According to the average stress criterion, fracture propagates whenever the average stress on a material length reaches the tensile strength. The material length is $(2/\pi) \times l_{ch}$ so that, for the problem under examination, the average stress criterion is repre-

sented by the second equation in the system (39), with $\delta = 2/\pi$, leading to:

$$\frac{K_{\mathrm{I}}^*}{K_{\mathrm{Ic}}^*} = \left[f_{\vartheta\vartheta}^{\mathrm{I}}(\vartheta) + \frac{\lambda_{\mathrm{I}}}{\lambda_{\mathrm{II}}} 4^{\lambda_{\mathrm{II}}-\lambda_{\mathrm{I}}} \tan\psi\, f_{\vartheta\vartheta}^{\mathrm{II}}(\vartheta) \right]^{-1} \tag{56}$$

where Eq. (26) have been used. Note that now the generalized fracture toughness is still given by Eq. (36), but with $\xi = \lambda_{\mathrm{I}} \times 4^{1-\lambda_{\mathrm{I}}}$ (Seweryn, 1994). The right hand side depends on ϑ; thus the actual critical mode I GSIF is the minimum one. The equation providing the crack deflection ϑ_{c} can be obtained differentiating Eq. (56); by means of Eq. (53) one gets:

$$f_{\mathrm{r}\vartheta}^{\mathrm{I}}(\vartheta) + \left[\frac{\lambda_{\mathrm{I}}}{\lambda_{\mathrm{II}}} \frac{1+\lambda_{\mathrm{II}}}{1+\lambda_{\mathrm{I}}} 4^{\lambda_{\mathrm{II}}-\lambda_{\mathrm{I}}} \right] \tan\psi\, f_{\mathrm{r}\vartheta}^{\mathrm{II}}(\vartheta) = 0 \tag{57}$$

It is worth observing that: (*i*) the classical $\sigma_{\vartheta\vartheta}$-max criterion (Erdogan and Sih, 1963) cannot be applied for notches, since the direction where the hoop stress is maximum varies with the radial coordinate, while it coincides with the average stress criterion for a crack ($\omega = 0°$); (*ii*) only for the crack case, i.e. when the term in the square brackets equals unity, the direction of crack propagation coincides with the direction where the (average) shearing stress vanishes, see Eq. (1c).

For the sake of comparison, in Fig. 11 we plot the crack deflection and the resistance domain for two notch opening angles (0° and 60°) according to the average stress criterion and FFM. Differences are small although not negligible: for instance, according to the former criterion ϑ_{IIc} is equal to $-70.5°$ for a crack ($\omega = 0°$) and equal to $-75.6°$ according to the latter criterion. From Fig. 11 it is seen that the average stress criterion generally tends to overestimate the failure load and to underestimate the crack deflection, i.e. FFM estimates are more conservative (and more reliable, in the authors' opinion). Here it is worth recalling that, for several geometries, FFM predictions have proved to be in almost perfect agreement with cohesive zone models predictions (Henninger et al., 2007; Cornetti et al., 2012).

8. Size effect and mode mixity

The introduction of a physical length against which to scale the notch tip GSIFs enables further aspects of the solution to be drawn out, such as the influence of a V-notch on the so-called size effect. Hence let us consider a set of self-similar geometries as the ones drawn in Fig. 12. Dimensional analysis allows us to write directly:

$$K_{\mathrm{I}}^* = f_{\mathrm{I}}(\omega, a/b)\sigma b^{1-\lambda_{\mathrm{I}}} \tag{58a}$$

$$K_{\mathrm{II}}^* = f_{\mathrm{II}}(\omega, a/b)\sigma b^{1-\lambda_{\mathrm{II}}} \tag{58b}$$

where σ is the nominal stress, b is a characteristic size of the structure and f_{I}, f_{II} are shape factors depending on the geometry, here synthetically defined by the notch opening angle ω and relative notch depth a/b. Upon substitution of Eq. (58) in the definition of G_0 and d_0 (Eq. (3)), Eq. (7) becomes:

$$\left.\begin{matrix} \sigma_{\mathrm{f}}/\sigma_{\mathrm{u}} \\ \vartheta_{\mathrm{c}} \end{matrix}\right\} = f\left(s, \omega, \frac{a}{b}\right) \tag{59}$$

where we introduced the brittleness number s as (Carpinteri, 1980, 1981, 1982):

$$s = \frac{K_{\mathrm{Ic}}}{\sigma_{\mathrm{u}}\sqrt{b}} = \sqrt{\frac{l_{\mathrm{ch}}}{b}} \tag{60}$$

Please note that a low brittleness number indicates markedly brittle behavior. Eq. (59) shows that geometrically similar V-notched structures present the same relative failure stress and crack deflection (i.e. they have the same structural behavior) provided they have the same brittleness number s; or, equivalently, two geometrically similar V-notched structures, made of the same material,

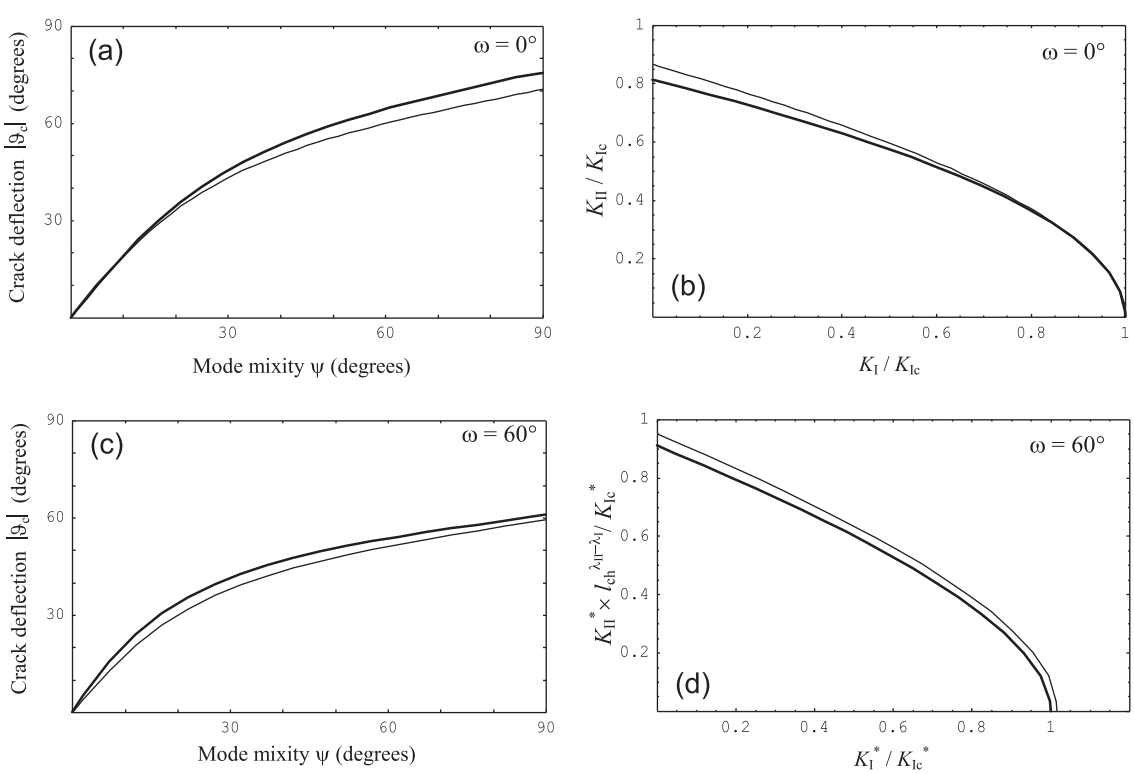

Fig. 11. Comparison between FFM (thick lines) and average stress (thin lines) predictions for a crack ($\omega = 0°$, a and b) and for a re-entrant corner ($\omega = 60°$, c and d). Note that, for a crack, FFM coincides with the G-max fracture criterion, whereas the average stress criterion coincides with the $\sigma_{\vartheta\vartheta}$-max fracture criterion (a–b). For the sake of comparison in (d) we normalized to the same generalized fracture toughness the critical GSIFs provided by both the approaches.

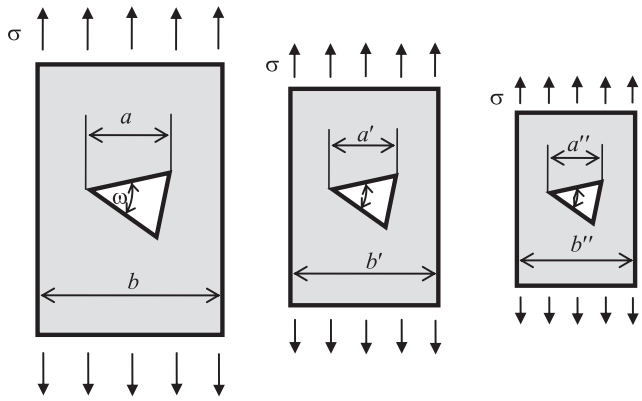

Fig. 12. Self-similar specimens with a re-entrant corner of amplitude ω.

behave differently. This is a fundamental difference with respect to LEFM crack problems (see Eq. (8)), where the failure load depends only on the fracture toughness (brittleness number comes into play only when LEFM is replaced by more refined models such as the cohesive crack model, see e.g. Carpinteri, 1989); on the other hand, even if critical conditions are sufficiently well described by the GSIFs alone, for notched geometries the solution *always* depends on s.

Now let us focus our attention to the size effect on the nominal stress at failure. If only the mode I GSIF is different from zero, failure will occur whenever the mode I GSIF reaches the generalized fracture toughness given by Eq. (36). According to Eq. (58a), the logarithm of the nominal stress at failure σ_f is given by Carpinteri (1987):

$$\ln \sigma_f = \ln \left[\frac{K^*_{Ic}}{f_I(\omega, a/b)} \right] - (1 - \lambda_I) \ln b \tag{61}$$

It means that the strength of a V-notched structure decreases according to a power law of the structural size with exponent $(1 - \lambda_I)$ or, equivalently, in a bi-logarithmic plot the strength vs. size curve is a straight line with (negative) slope equal to $(1 - \lambda_I)$, see Fig. 13(a).

If the V-notched structure is under pure mode II loading, failure will occur whenever the mode II GSIF reaches its critical value given by Eq. (45). Accordingly, the size effect is given by:

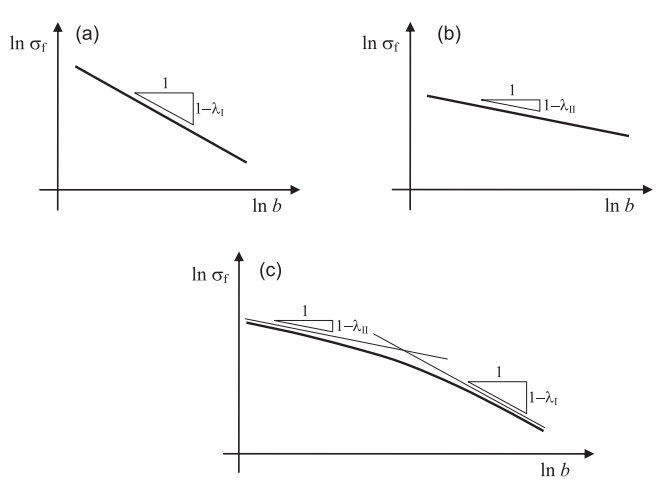

Fig. 13. Size effect on nominal stress at failure: (a) pure mode I loading; (b) pure mode II loading; (c) mixed mode loading.

$$\ln \sigma_f = \ln \left[\frac{K^*_{IIc}}{f_{II}(\omega, a/b)} \right] - (1 - \lambda_{II}) \ln b \tag{62}$$

i.e. in the bi-logarithmic plot the strength vs. size curve is a straight line with (negative) slope equal to $(1 - \lambda_{II})$, see Fig. 13(b). Since $\lambda_{II} > \lambda_I$, the size effect is stronger under mode I than under mode II loadings.

In the case of mixed mode loadings, we have to substitute both Eq. (58) into the stress condition (27) for crack propagation. Accordingly, we get:

$$\frac{\sigma_f}{\sigma_u} = \frac{1}{f_I(\omega, a/b)\left[\bar{f}^I_{\vartheta\vartheta}/\delta^{1-\lambda_I}\right]\left(\frac{b}{l_{ch}}\right)^{1-\lambda_I} + f_{II}(\omega, a/b)\left[\bar{f}^{II}_{\vartheta\vartheta}/\delta^{1-\lambda_{II}}\right]\left(\frac{b}{l_{ch}}\right)^{1-\lambda_{II}}} \tag{63}$$

The terms in square brackets show a modest variation with the size, so that the terms in round brackets dominate in Eq. (63). It means that, for large sizes and/or brittle materials, the first addend at the denominator (i.e. mode I) prevails; on the other hand, for small sizes and/or less brittle materials, the second addend at the denominator (i.e. mode II) does govern the problem. By means of Eqs. (60), Eq. (63) can be rewritten as:

$$\frac{\sigma_f}{\sigma_u} = \frac{1}{f_I(\omega, a/b)\left[\bar{f}^I_{\vartheta\vartheta}/\delta^{1-\lambda_I}\right] s^{-2(1-\lambda_I)} + f_{II}(\omega, a/b)\left[\bar{f}^{II}_{\vartheta\vartheta}/\delta^{1-\lambda_{II}}\right] s^{-2(1-\lambda_{II})}} \tag{64}$$

The presence of the brittleness number s in (64) highlights that the transition from mode I-to mode II-governed failure depends both on size and material brittleness. Thus we conclude that the size effect for a V-notched structure under mixed mode loading is represented by a curve with two slant asymptotes in the bilogarithmic plot (see Fig. 13(c)): the right one with slope $-(1 - \lambda_I)$, the left one with slope $-(1 - \lambda_{II})$. This is a general trend, i.e. independent of the geometry and fracture criterion adopted.

It is worth observing that the analysis of the mode mixity leads to the same conclusion. In fact substitution of Eq. (58) into Eq. (9) provides:

$$\begin{aligned} \psi &= \arctan \left[\frac{f_{II}(\omega, a/b)}{f_I(\omega, a/b)} \left(\frac{l_{ch}}{b} \right)^{\lambda_{II} - \lambda_I} \right] \\ &= \arctan \left[\frac{f_{II}(\omega, a/b)}{f_I(\omega, a/b)} s^{2(\lambda_{II} - \lambda_I)} \right] \end{aligned} \tag{65}$$

Eq. (65) clearly shows that, except in the crack case ($\lambda_I = \lambda_{II} = 1/2$), the mode mixity does not depend only on the shape factors, but also on the brittleness number, i.e. on the structural size. In fact, whatever is the ratio between f_{II} and f_I (provided they are both different from zero), for sufficiently large sizes the mode mixity will always tend to zero (i.e. pure mode I), whereas it will tend to $\pi/2$ for vanishing sizes (i.e. pure mode II).

While the large-size asymptote is always physically meaningful, the small-size asymptote could become only theoretical if mode II prevails for sizes too small for the asymptotic approach to hold true. In fact, when the finite crack extension is not negligible with respect to the other geometrical dimensions (e.g. for very small sizes), disregarding higher order terms in the asymptotic stress field is not acceptable. Similarly to LEFM, the asymptotic approach to V-notched structures leads to an infinite strength for vanishing sizes, i.e. to a result that, within the present coupled Rankine-Griffith criterion and under constant remote tensile stresses (see Fig. 12), must be regarded as physically unacceptable.

For the sake of simplicity, in the following we will consider only geometries with a unique relevant geometrical dimension, the notch depth a (i.e. $b \gg a$), so that a itself can be seen as a measure of the structural size, and the brittleness number is therefore equal to $s = K_{Ic}/\sigma_u\sqrt{a}$. Accordingly, Eqs. (58) and (65) become:

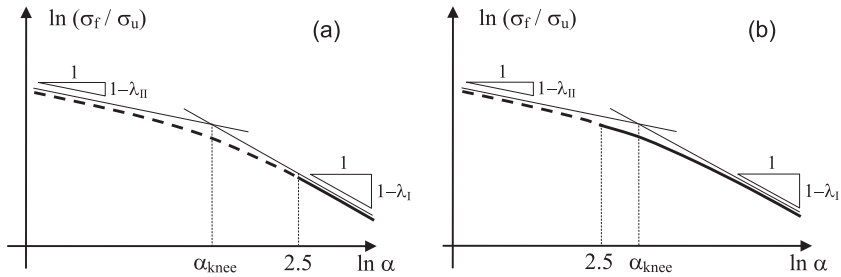

Fig. 14. Size effect on nominal stress at failure under mixed mode loadings: failure occurring always (i.e. within the range of validity of the asymptotic approach) in prevailing mode I (a); failure occurring effectively in mixed mode (b). The dashed part of the curves is only theoretical, since beneath the 2.5 limit value the asymptotic analysis may be not reliable.

$$K_{\mathrm{I}}^{*} = \Lambda_{\mathrm{I}} \sigma a^{1-\lambda_{\mathrm{I}}} \tag{66a}$$

$$K_{\mathrm{II}}^{*} = \Lambda_{\mathrm{II}} \sigma a^{1-\lambda_{\mathrm{II}}} \tag{66b}$$

$$\psi = \arctan\left[\frac{\Lambda_{\mathrm{II}}}{\Lambda_{\mathrm{I}}} \frac{1}{\alpha^{\lambda_{\mathrm{II}}-\lambda_{\mathrm{I}}}}\right] = \arctan\left[\frac{\Lambda_{\mathrm{II}}}{\Lambda_{\mathrm{I}}} s^{2(\lambda_{\mathrm{II}}-\lambda_{\mathrm{I}})}\right] \tag{66c}$$

where Λ_{I} and Λ_{II} are constant factor to be determined by a FEA together with a suitable procedure like the reciprocal work contour integral method (Carpenter, 1984; Sinclair et al., 1984) and $\alpha = a/l_{\mathrm{ch}}$ is the dimensionless notch depth or structural size (note that $\alpha = 1/s^2$). It is evident the relevance of the brittleness number s, which univocally determine the mode mixity ψ. By means of Eq. (66a) and Eq. (36), the equation of the large-size asymptote becomes:

$$\frac{\sigma_{\mathrm{f}}}{\sigma_{\mathrm{u}}} = \frac{\xi}{\Lambda_{\mathrm{I}}} \frac{1}{\alpha^{1-\lambda_{\mathrm{I}}}} \tag{67}$$

while the equation of the small-size asymptote is, by means of Eqs. (66b) and (45):

$$\frac{\sigma_{\mathrm{f}}}{\sigma_{\mathrm{u}}} = \frac{\xi\eta}{\Lambda_{\mathrm{II}}} \frac{1}{\alpha^{1-\lambda_{\mathrm{II}}}} \tag{68}$$

The abscissa of the point of intersection of the two asymptotes defines the notch size a_{knee} at which the failure load curve shows a knee (see Fig. 14):

$$\alpha_{\mathrm{knee}} = \frac{a_{\mathrm{knee}}}{l_{\mathrm{ch}}} = \left(\frac{\Lambda_{\mathrm{II}}}{\Lambda_{\mathrm{I}}\eta}\right)^{\frac{1}{\lambda_{\mathrm{II}}-\lambda_{\mathrm{I}}}} \tag{69}$$

In other words, for dimensionless notch size $\alpha \ll \alpha_{\mathrm{knee}}$ failure occurs in prevailing mode II; for $\alpha \gg \alpha_{\mathrm{knee}}$ failure occurs in prevailing mode I; for intermediate values it occurs effectively in mixed mode. As already observed, the present asymptotic approach works only if the finite crack advancement falls within the GSIF-dominated zone at the notch tip. Since the length of the finite crack growth is always less than 0.637 l_{ch} (see Section 5), we can assume the previous requirement to be fulfilled if the usual condition for small scale yielding in LEFM problems holds:

$$a > 2.5\left(\frac{K_{\mathrm{Ic}}}{\sigma_{\mathrm{u}}}\right)^2 = 2.5 l_{\mathrm{ch}}, \text{ i.e. } \alpha > 2.5 \tag{70}$$

implying that the crack advancement is always less than about $a/4$. Although the requirement provided by Eq. (70) should be seen as a reference value, since the weight of higher order terms in the asymptotic stress field expansion may vary from geometry to geometry, it is worth observing that the region dominated by the first terms in the stress field asymptotic expansion (Eq. (1)) ahead of the notch tip is usually larger than the corresponding one in front of a crack (Dunn et al., 1997c; Strandberg, 2002), so that the limitation (70) can be considered as conservative.

Taking the lower limit (70) into account, for a generic structure with a re-entrant corner subjected to mixed mode we can have two possible scenarios: (*i*) $\alpha_{\mathrm{knee}} \ll 2.5$, i.e. the mode II contribution to failure is always negligible and the failure of the V-notched structure is simply attained when K_{I}^{*} reaches K_{Ic}^{*} (Fig. 14(a)); (*ii*) $\alpha_{\mathrm{knee}} \approx 2.5$ or $\alpha_{\mathrm{knee}} > 2.5$. In this latter case (Fig. 14(b)) failure occurs effectively in mixed mode, the mode II contribution being no more negligible, although its effect diminishes as the structural size or material brittleness increases ($\alpha \to \infty$). In the next section we will consider two geometries, one for each scenario.

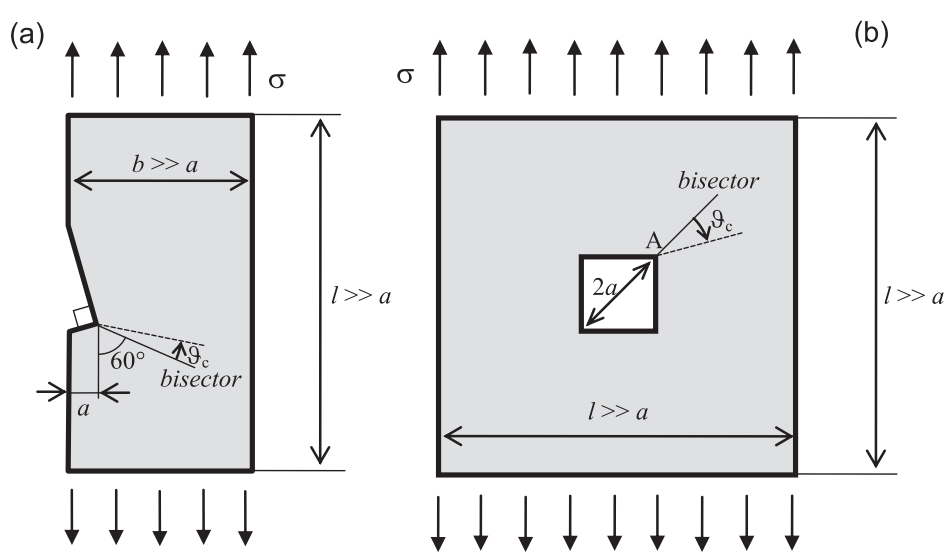

Fig. 15. Edge V-notched (a) and square holed (b) plates under uniform remote uniaxial tension. The direction of the V-notch emanated crack is marked by a dashed line.

Note that an investigation of the size effect on V-notched structures, based on the cohesive crack model and covering the whole range of sizes (i.e. including the small size flat asymptote, equal to $\sigma_f = \sigma_u$ for infinite or semi-infinite geometries under remote tensile loads) can be found in Bažant and Yu (2006). However their analysis is limited to mode I loadings.

9. Application to example problems

As example problems, we chose the same problems considered in Hills and Dini (2011), since highly representative. Furthermore, this choice allows a direct comparison between the plastic zone shape analysis performed in Hills and Dini (2011) and the present fracture mechanics investigation.

9.1. Geometry 1

Let us consider a semi-infinite plate with a 90°-edge notch, whose bisector is inclined of 60° with respect to the edge (see Fig. 15(a)), under a remote uniaxial tensile stress σ; a is the notch depth. The corresponding eigenvalues can be found in the first two columns of Table 1 (for $\omega = 90°$). By some suitable technique coupled to a linear elastic FEA of the problem, it is possible to extract the values of the Λ_I and Λ_{II} factors providing the GSIFs (Eq. (66a,b)):

$$\Lambda_I = 2.134, \quad \Lambda_{II} = 0.387 \tag{71}$$

Actually, we took these values from Hills and Dini (2011) and adapted them to the current definition of GSIFs (see Eq. (1)). Substitution of Eq. (66a,b) into the notch driving force definition (Eq. (3)) yields:

$$G_0 = 0.252\,\sigma \tag{72}$$

Exploiting the η value given in Table 1 (for $\omega = 90°$), from Eq. (69) one finds $\alpha_{knee} = 0.0121$. This value is much smaller than 2.5. Therefore we can immediately conclude that failure occurs always in prevailing mode I. To check this statement we have simply to compute the mode mixity ψ for different dimensionless notch sizes α (larger than 2.5) by Eq. (66c), see Fig. 16(a); we find values smaller than 7.4° (obtained for $\alpha = 2.5$), denoting that fracture propagation is clearly mode I in character. Then the analysis performed in Section 5 (e.g. Table 3) provides the critical value G_{0f} of the notch driving force (as well as the crack deflection ϑ_c), and Eq. (72) finally yields the value of the remote stress σ_f at failure (the same value can be obtained by the analysis provided in Section 6, where the critical values of the GSIFs are given). The results are plotted in Fig. 16(b). Since the failure stress values provided by the present analysis lay almost perfectly on the mode I asymptote, we conclude that, at least for what concerns the failure load, the error done in disregarding the mode II contribution is effectively negligible (less than 3.3%, obtained for $\alpha = 2.5$).

Fig. 16(c) shows how the crack deflection decreases as the dimensionless structural size increases. Although the direction ϑ_c of crack propagation is not large ($0° < \vartheta_c < 16.6°$), meaning that the V-notch emanated crack tends to grow along the notch bisector with a small deflection towards the direction perpendicular to the remote uniaxial stress field (see Fig. 15(a)), it is interesting to observe that, for small a/l_{ch} values, ϑ_c values are not negligible: that is, for the present geometry, the mode II contribution provides an effect on the failure load which is always negligible, at least from an engineering point of view, while this is not the case for what concerns the direction of crack propagation.

9.2. Geometry 2

Let us consider an infinite plate with a square hole, with diagonal $2a$, under a remote uniaxial tensile stress σ aligned along the square sides (see Fig. 15(b)). There are four V-notches, all under the same stress state for symmetry reasons. The re-entrant corner amplitude is 90° also in this case, so that the eigenvalues and the η

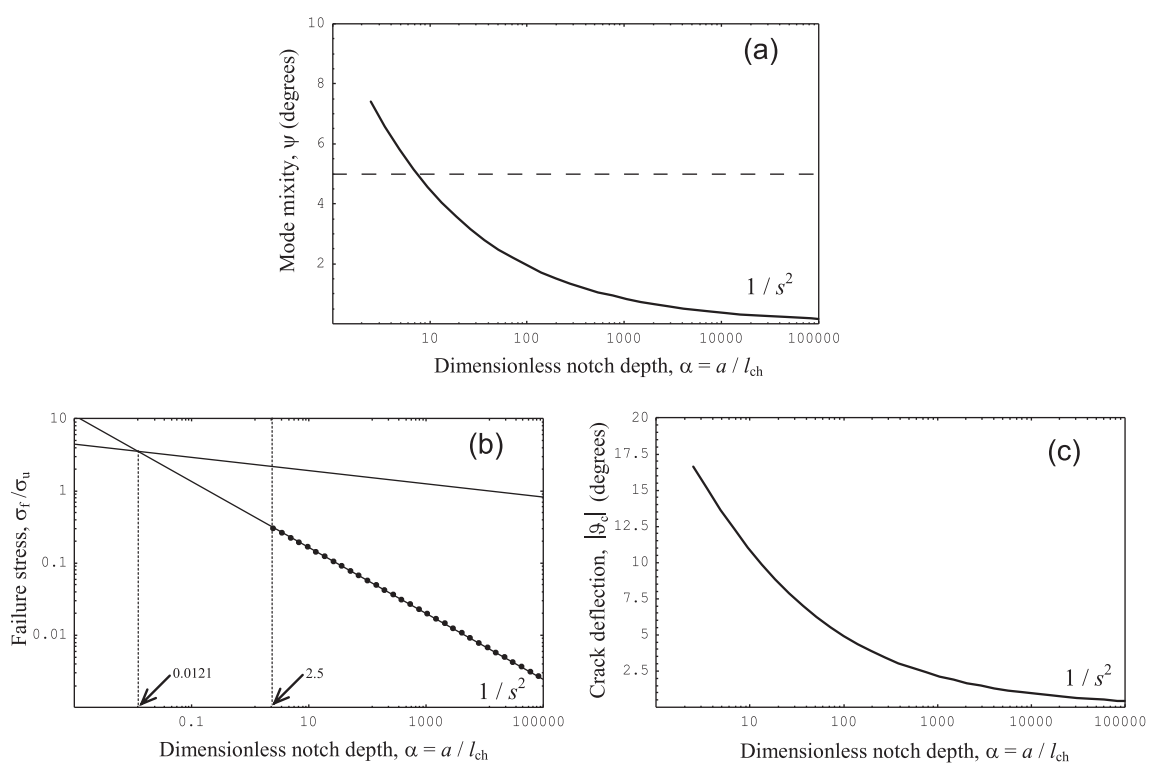

Fig. 16. Mode mixity (a), failure stress (b) and crack deflection (c) vs. structural size (dimensionless plots) for Geometry 1. In (b) the continuous lines represent the mode I and mode II asymptotes, while the dots are the present model predictions.

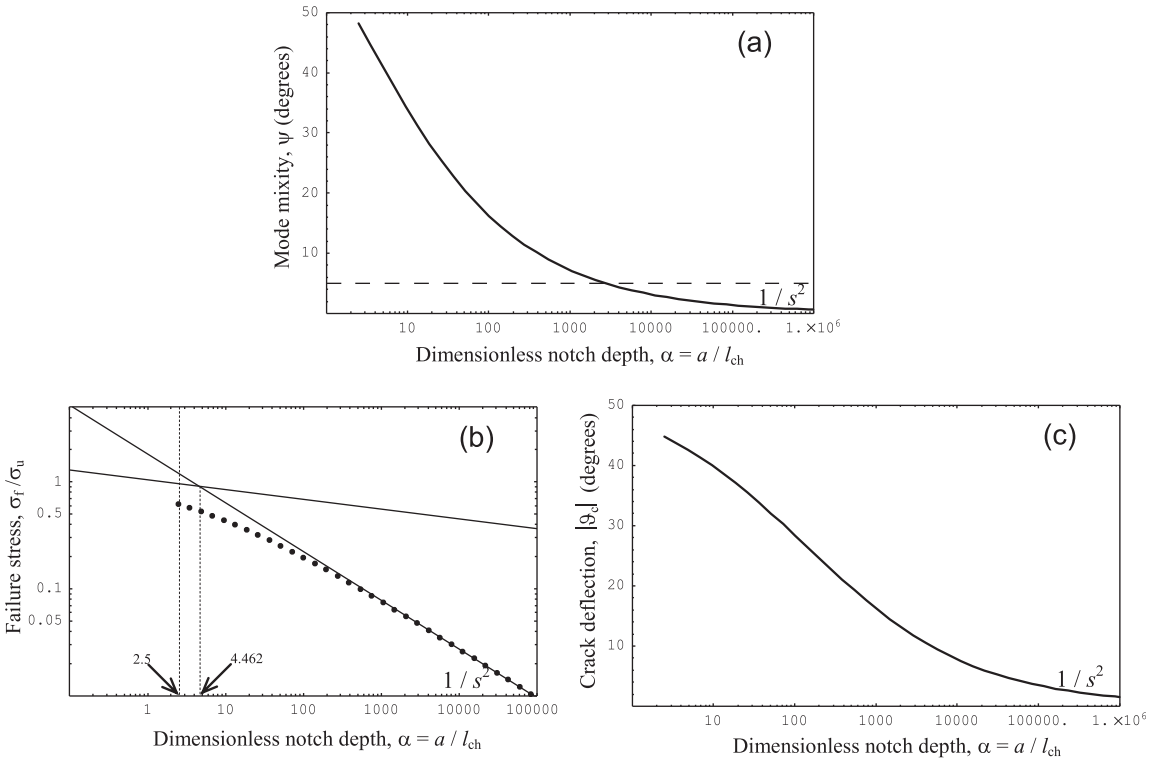

Fig. 17. Mode mixity (a), failure stress (b) and crack deflection (c) vs. structural size (dimensionless plots) for Geometry 2. In (b) the continuous lines represent the mode I and mode II asymptotes, while the dots are the present model predictions.

value coincide with the ones of Geometry 1. Since the plate external dimensions are assumed to be much larger than the hole size, the GSIFs are given by Eq. (66), where the Λ_I,Λ_{II} factors can be extracted by a FEA analysis (Hills and Dini, 2011), yielding:

$$\Lambda_I = 0.551, \quad \Lambda_{II} = 0.858 \tag{73}$$

from which (Eq. (3)):

$$G_0 = 0.959\sigma \tag{74}$$

The square hole size characterizing the transition between mode I and mode II crack propagation is now $\alpha_{knee} = 4.462$ (from Eq. (69)). This value is larger than 2.5. It means that, generally, failure occurs really in mixed mode, i.e. the mode II contribution cannot be neglected. This conclusion can be checked by directly computing the failure load, as we did for the previous geometry. Varying the dimensionless notch size α, we find mode mixity angles ψ in the range 0°-48° by Eq. (66c), see Fig. 17(a). For each ψ value, the analysis in Section 5 or 6 provides the critical value of the GSIFs and, consequently, the nominal stress at failure can be achieved either by Eq. (66) or (74). The results are plotted in Fig. 17(b). It is clear that the failure stress significantly deviates from the mode I asymptote for diminishing hole sizes, when the failure load estimates tend to (although not reaching) the mode II asymptote. Only for square hole sizes a larger than about 3000 times the characteristic length l_{ch} (when ψ becomes smaller than 5°, see Fig. 17(a)) one can neglect the mode II contribution, making an error less than 2%.

Fig. 17(c) shows how the crack deflection ϑ_c decreases as the dimensionless square hole size increases. It is evident that, for this geometry, crack deflections are typically relevant. Note however

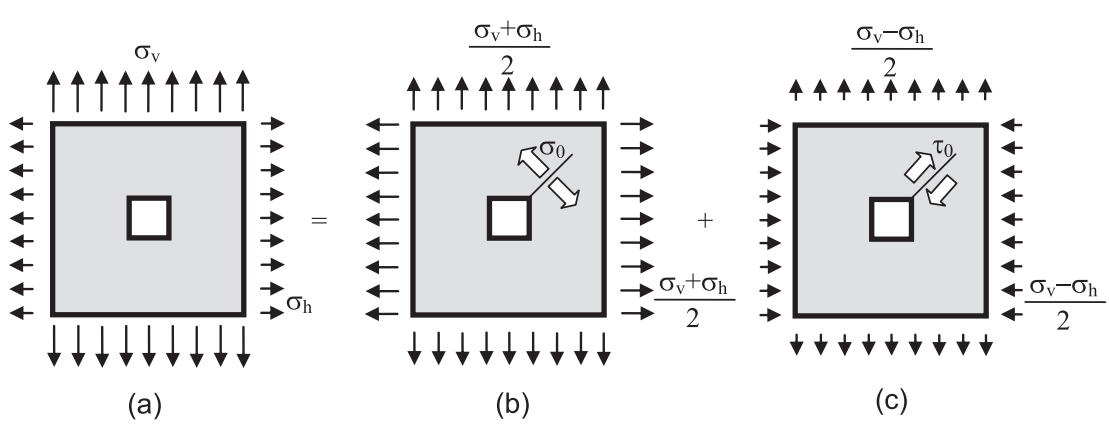

Fig. 18. Square holed plates under a bi-axial stress field (a) decomposed into an hydrostatic (b) and a pure shear (c) component. For loading (b) notches are subjected to pure mode I and to pure mode II for loading (c).

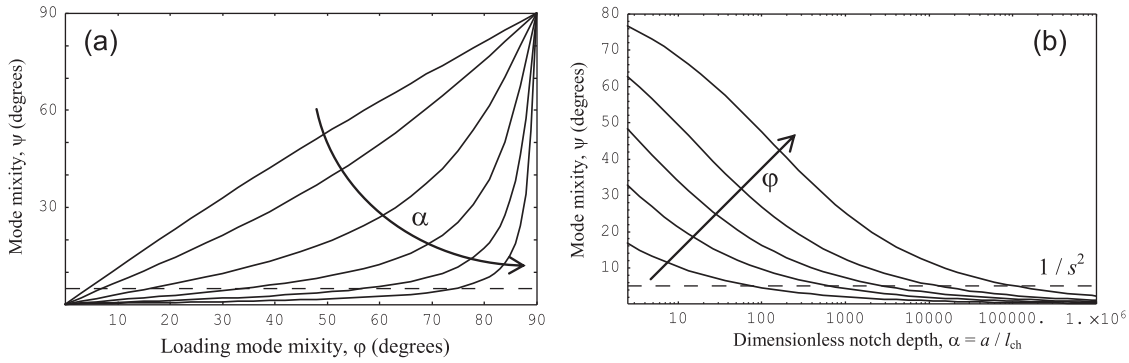

Fig. 19. Mode mixity ψ vs. loading mode mixity φ for $\alpha = 2.5$, 10, 10^2, 10^3, 10^4, 10^5 (a) and vs. dimensionless size α for $\varphi = 15°$, 30°, 45°, 60°, 75° (b). The dashed line corresponds to $\psi = 5°$, i.e. the value below which mode II can be considered negligible.

that the deviation from the bisector remains smaller than the value corresponding to the direction perpendicular to the uniaxial remote tensile stress field (i.e. 45°), see Fig. 15(b).

9.3. Geometry 3

The last example problem we are going to analyze has the same geometry of example 2 but two independent loads, namely the vertical remote tensile stress σ_v and the horizontal remote stress σ_h (see Fig. 18). Without loss of generality, we can assume $\sigma_v \geqslant \sigma_h$. Letting σ_h vary from $-\sigma_v$ to $+\sigma_v$, the mode I GSIF is always non-negative. It is worth noting that, varying the ratio of the vertical to the normal remote stress from + 1 to − 1, the loading continuously varies from pure mode I to pure mode II. In fact, as evidenced in Fig. 18, the load can be decomposed into the sum of two sets of loads: the former is represented by a remote hydrostatic tensile stress field $\sigma_0 = (\sigma_v + \sigma_h)/2$, the latter by a remote shearing stress field $\tau_0 = (\sigma_v - \sigma_h)/2$ oriented along the square diagonals. Symmetry reasons allow one to state that the set in Fig. 18(b) corresponds to a pure mode I loading, whereas the set in Fig. 18(c) corresponds to a pure mode II loading. In other words, in terms of σ_0 and τ_0 the fracture modes are uncoupled.

These considerations suggest to introduce the parameter φ defining the *loading* mode mixity as:

$$\tan\varphi = \frac{\tau_0}{\sigma_0} = \frac{\frac{\sigma_v}{\sigma_h} - 1}{\frac{\sigma_v}{\sigma_h} + 1} \tag{75}$$

so that $\varphi = 0$ (i.e. $\tau_0 = 0$ or $\sigma_v = \sigma_h$) corresponds to pure mode I and $\varphi = \pi/2$ (i.e. $\sigma_0 = 0$ or $\sigma_h = -\sigma_v$) corresponds to pure mode II. Note that tan (φ) can be seen as the ratio between the normal and shear component of the resultant force acting on the notch bisector. However it is important to emphasize that, for notched structures, the (*effective*) mode mixity ψ does not coincide with the *loading* mode mixity φ. In fact, for what we saw in the previous sections, we expect that the mode mixity depends on the loading mode mixity as well as on the brittleness number. To highlight this dependency, we have simply to observe that the GSIFs are given by:

$$K_I^* = \Lambda_I\ \sigma_0\ a^{1-\lambda_I} \tag{76a}$$

$$K_{II}^* = \Lambda_{II}\ \tau_0\ a^{1-\lambda_{II}} \tag{76b}$$

Since the present Geometry 3 can be seen as the superposition of two Geometry 2 cases, the Λ_I,Λ_{II} factors are simply twice the values given in Eq. (73), i.e. $\Lambda_I = 1.102$ and $\Lambda_{II} = 1.717$, while the eingenvalues λ_I,λ_{II} coincide with the ones of the previous geometries, ω being still equal to 90°. On the other hand, Geometry 2 can be seen as a particular case of Geometry 3 when $\sigma_0 = \tau_0 = \sigma/2$ (implying $\varphi = \pi/4$). Upon substitution of Eq. (76) into Eqs. (3) and (9) respectively, we get:

$$G_0 = 1.919(\tan\varphi)^{1.251}\sigma_0 \tag{77a}$$

$$\psi = \arctan\left(\frac{1.558\tan\varphi}{\alpha^{0.364}}\right) = \arctan(1.558\, s^{0.728}\tan\varphi) \tag{77b}$$

Eq. (77b) clearly shows that ψ does not coincide with φ, since the mode mixity ψ affecting the V-notch depends also on size and material brittleness, as Fig. 19(a) highlights. More in detail, Fig. 19(a) shows the ψ vs. φ plots for different sizes: only for relatively small sizes the loading and effective mode mixity are approximately equal. For larger size, $\psi < \varphi$, i.e. the influence of mode I on crack propagation is higher with respect to what one could expect from the normal to shear stress ratio. This trend is stronger for larger sizes. For very large sizes (or very brittle materials) the transition from mode I to mode II occurs, very sharply, only for loading

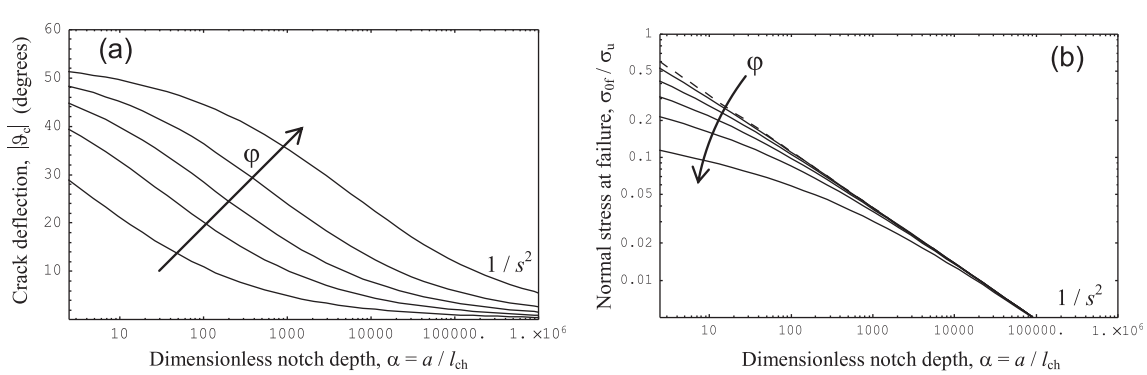

Fig. 20. Crack deflection $|\vartheta_c|$ (a) and dimensionless critical hydrostatic stress σ_{0f} (b) vs. dimensionless size α for $\varphi = 15°$, 30°, 45°, 60°, 75°. In (b) the dashed line corresponds to the failure load estimates if only the mode I contribution is taken into account, i.e. a straight line with negative slope $-(1-\lambda_I)$.

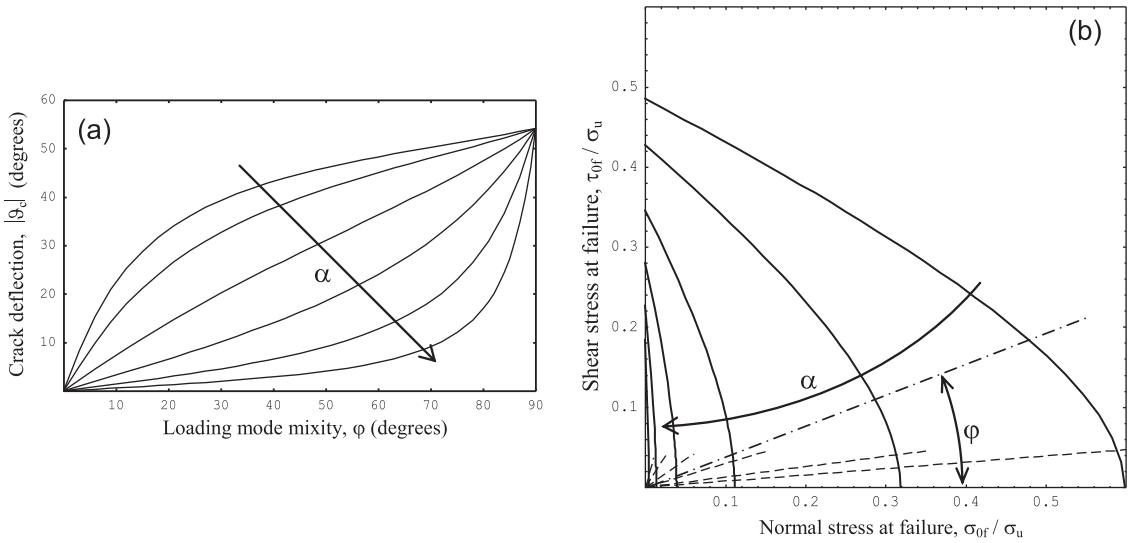

Fig. 21. Crack deflection $|\vartheta_c|$ vs. loading mode mixity φ (a) and dimensionless critical stresses σ_{0f},τ_{0f} (b) for α = 2.5, 10, 10^2, 10^3, 10^4, 10^5. In (b) the dot-dashed line denotes a possible loading path, whose inclination is the loading mode mixity φ. The slopes of the dashed lines correspond to φ values below which the mode II contribution to the failure load can be neglected according to the different α values.

mode mixities close to 90°. The intercepts with the ψ = 5° straight line denote the φ values below which the failure load can be computed as if the structure were loaded in pure mode I. This threshold φ value increases with the dimensionless size. On the other hand, in Fig. 19(b) we plotted ψ vs. α for different loading mode mixity φ: it is seen that failure tends to occur in mode I for large size whatever is the loading mode mixity; of course, the smaller is φ, the faster is the transition towards mode I failure. In this latter case the intercepts with the ψ = 5° straight line denote the α value over which the mode II contribution to the failure load can be neglected. Of course, this threshold α value increases with loading mode mixity.

For a given α and φ value, ψ is computed by Eq. (77b). Then, by the analysis in either Section 5 or 6, we can obtain the crack deflection and the critical value of either the notch driving force or the mode I GSIF. Finally, the value of σ_0 (or τ_0) at failure are obtained by Eq. (76) or (77a). Results are plotted in Fig. 20(a,b) versus the (dimensionless) structural size for different values of the loading mode mixity φ. For what concerns the crack deflection, Fig. 20(a) shows it diminishes increasing the size or the material brittleness, i.e. it does not depend only on loading mode mixity; obviously, it is higher for larger loading mode mixity values. For what concerns the remote hydrostatic stress at failure, Fig. 20(b) shows that, for $\alpha \to \infty$, it tends to the mode I asymptote for any loading mode mixity φ value. Nevertheless it is seen that the size at which the curve matches the asymptote increases along with the loading mode mixity. A straightforward analysis shows in fact that the abscissa of the knee of the curves is, for the present two-load set:

$$\alpha_{\text{knee}} = \frac{a_{\text{knee}}}{l_{\text{ch}}} = (1.723 \tan \varphi)^{2.747} \tag{78}$$

which depends on φ, tending to zero or infinite for pure mode I and pure mode II loadings respectively.

In Fig. 21 the crack deflection and the resistance domain are plotted vs. the loading mode mixity φ for different values of the size. For what concerns the crack deflection (Fig. 21(a)), it is worth observing that it increases from zero to the mode II limit value (~54°, valid for the 90° re-entrant corners) for any size. However, the transition occurs mainly at low φ values for small sizes, while it takes place at high φ values for large sizes.

In Fig. 21(b), instead of plotting the critical value of the hydrostatic stress vs. φ for different values of the size, it is more significant to draw in the (σ_0,τ_0) plane the points whose coordinates are the couple of critical stresses, normal and shearing respectively. The plot thus obtained represents the resistance domain, i.e. the points below the line represent admissible stress states, while points lying above represent stress states causing crack propagation. Note that the inclination of the straight line connecting a given point on the failure curve with the origin is now the loading mode mixity φ. Different curves correspond to different sizes. It is worth observing that the intercept with the σ_0-axis, i.e. the normal stress at failure in mode I, scales as $\alpha^{-(1-\lambda_I)}$, whereas the intercept with the τ_0-axis, i.e. the shear stress at failure in mode II, scales as $\alpha^{-(1-\lambda_{II})}$. Being $\lambda_{II} > \lambda_I$, the critical normal stress in mode I diminishes with the size more rapidly if compared with the critical shear stress in mode II. As a consequence, the shape of the resistance domain changes by varying the size, the (negative) slope becoming steeper and steeper as the size increases. This behaviour simply confirms that the failure load is not affected by shear stress to normal stress ratio values below a certain threshold, which increases as the size increases. The dashed line correspond to loading mixity values φ (computed by Eq. (77b) setting ψ = 5°) under which the mode II contribution to the failure load can be neglected.

The examples herein considered are mainly theoretical. A comparison with a broad set of experimental data can be found in Sapora et al. (2013). Here we want just to observe that most of the results available in the literature about V-notched structure under mixed-mode loading refer to double edge V-notched specimens (the so-called Arcan test, e.g. Seweryn et al., 1997). Failure load predictions are usually given vs. loading mode mixity, i.e. vs. the ratio between normal and shear components of the resultant force over the notch bisector (that is, the ligament). However, as the results in Fig. 21 clearly highlight, such diagrams are limited to a specific material since there is not a one-to-one relationship between the dimensionless failure load (or the crack deflection) and the loading mode mixity.

10. Conclusions

In the present paper we applied the FFM criterion provided in Cornetti et al. (2006) to determine the critical load in V-notched structures under combined Mode I and Mode II loadings. With re-

spect to simple Mode I loadings (Carpinteri et al., 2008), the mixed mode problem is more complex since, beyond the failure load, also the direction of the crack onset at the re-entrant corner tip is unknown. Nevertheless, exploiting suitable weight functions for the SIFs of a V-notch-emanated crack (Beghini et al., 2007), we were able to formulate the model as a standard minimization-under-constraint problem and to solve it by means of the Lagrange multiplier technique.

In mixed-mode loading cases, we showed that our model is able to explain the growing relevance of the mode II contribution for increasing material lengths l_{ch}, while it is negligible if l_{ch} tends to zero. Nevertheless, since the present approach is based on the asymptotic stress field, it yields accurate results only for sufficiently small l_{ch} values (with respect to the other geometrical dimensions, e.g. the notch/hole size in the examples of Section 9). If this condition is not met, it is necessary to consider further terms in the stress field asymptotic expansions (see, e.g., Cheng et al., 2012 where the maximum circumferential stress criterion is exploited) or to tackle the problem numerically (see, e.g., Hebel et al. (2010) for what concerns the FFM criterion).

The results of the model have been given both in a traditional form, i.e. in terms of the GSIFs, and according to a new formalism introduced by Hills and Dini (2011), i.e. in terms of the notch driving force. Numerical values of the crack deflection and of the critical quantities have been carefully computed and tabulated in order to be of help in engineering practice. A detailed analysis of limit cases has been also provided aiming to point out that the present model matches classical LEFM results.

In the second part of the paper, the size effect on the strength of a structure containing a re-entrant corner has been deeply investigated: differently from what occurs in cracked geometries, in the bi-logarithmic plot the size effect law is represented by a curve with two slant asymptotes whose slopes are related to Williams' Mode I and Mode II eigenvalues. We finally applied the model to compute the failure stress and the crack deflection for three simple structures, highlighting a general method to distinguish whether, in mixed mode problems, the effect of Mode II can be neglected or must be taken into account.

Appendix A. Williams' solution

For a re-entrant corner in an infinite homogeneous elastic medium (Fig. 1(a)) the asymptotic stress field is given by Eq. (1). The λ_I and λ_{II} eigenvalues refer to symmetric (mode I) and anti-symmetric loadings (mode II), respectively. They are the lowest roots of the two following equations, respectively:

$$\lambda \sin(2\gamma) + \sin(2\lambda\gamma) = 0 \tag{A.1}$$

$$\lambda \sin(2\gamma) - \sin(2\lambda\gamma) = 0 \tag{A.2}$$

The angular functions (eigenvectors) in Eq. (1) have the following expressions:

$$f^{I}_{rr}(\vartheta) = \frac{\cos[(\lambda_I-1)\gamma]\cos[(\lambda_I+1)\vartheta] - \frac{\lambda_I-3}{\lambda_I+1}\cos[(\lambda_I+1)\gamma]\cos[(\lambda_I-1)\vartheta]}{\cos[(\lambda_I+1)\gamma] - \cos[(\lambda_I-1)\gamma]} \tag{A.3}$$

$$f^{I}_{\vartheta\vartheta}(\vartheta) = \frac{\cos[(\lambda_I-1)\gamma]\cos[(\lambda_I+1)\vartheta] - \cos[(\lambda_I+1)\gamma]\cos[(\lambda_I-1)\vartheta]}{\cos[(\lambda_I-1)\gamma] - \cos[(\lambda_I+1)\gamma]} \tag{A.4}$$

$$f^{I}_{r\vartheta}(\vartheta) = \frac{\sin[(\lambda_I-1)\gamma]\sin[(\lambda_I+1)\vartheta] - \sin[(\lambda_I+1)\gamma]\sin[(\lambda_I-1)\vartheta]}{\sin[(\lambda_I-1)\gamma] - \frac{\lambda_I+1}{\lambda_I-1}\sin[(\lambda_I+1)\gamma]} \tag{A.5}$$

for mode I, and:

$$f^{II}_{rr}(\vartheta) = \frac{\sin[(\lambda_{II}-1)\gamma]\sin[(\lambda_{II}+1)\vartheta] - \frac{\lambda_{II}-3}{\lambda_{II}+1}\sin[(\lambda_{II}+1)\gamma]\sin[(\lambda_{II}-1)\vartheta]}{\sin[(\lambda_{II}-1)\gamma] - \frac{\lambda_{II}-1}{\lambda_{II}+1}\sin[(\lambda_{II}+1)\gamma]} \tag{A.6}$$

$$f^{II}_{\vartheta\vartheta}(\vartheta) = \frac{\sin[(\lambda_{II}-1)\gamma]\sin[(\lambda_{II}+1)\vartheta] - \sin[(\lambda_{II}+1)\gamma]\sin[(\lambda_{II}-1)\vartheta]}{-\sin[(\lambda_{II}-1)\gamma] + \frac{\lambda_{II}-1}{\lambda_{II}+1}\sin[(\lambda_{II}+1)\gamma]} \tag{A.7}$$

$$f^{II}_{r\vartheta}(\vartheta) = \frac{\cos[(\lambda_{II}-1)\gamma]\cos[(\lambda_{II}+1)\vartheta] - \cos[(\lambda_{II}+1)\gamma]\cos[(\lambda_{II}-1)\vartheta]}{\cos[(\lambda_{II}-1)\gamma] - \cos[(\lambda_{II}+1)\gamma]} \tag{A.8}$$

for mode II.

References

Barroso, A., Vicentini, D., Mantič, V., París, F., 2012. Determination of generalized fracture toughness in composite multimaterial closed corners with two singular terms – Part I: test proposal and numerical analysis. Engineering Fracture Mechanics 89, 1–14.

Bažant, Z.P., Yu, Q., 2006. Size effect on strength of quasibrittle structures with re-entrant corners symmetrically loaded in tension. Journal of Engineering Mechanics-ASCE 132, 1168–1176.

Beghini, M., Bertini, L., Di Lello, R., Fontanari, V., 2007. A general weight function for inclined cracks at sharp V-notches. Engineering Fracture Mechanics 74, 602–611.

Berto, F., Lazzarin, P., Kotousov, A., Harding, S., 2011. Out-of-plane singular stress fields in V-notched plates and welded lap joints induced by in-plane shear load conditions. Fatigue & Fracture of Engineering Materials & Structures 34, 291–304.

Camanho, P.P., Erçin, G.H., Catalanotti, G., Mahdi, S., Linde, P., 2012. A finite fracture mechanics model for the prediction of the open-hole strength of composite laminates. Composites: Part A 43, 1219–1225.

Carpenter, W.C., 1984. Calculation of fracture parameters for a general corner. International Journal of Fracture 24, 45–58.

Carpinteri, A., 1980. Size effect in fracture toughness testing: a dimensional analysis approach. In: Sih, G.C., Mirabile, M. (Eds.), Conference on Analytical and Experimental Fracture Mechanics, Rome, Italy, Sijthoff and Noordhoff, pp. 785–797.

Carpinteri, A., 1981. Static and energetic fracture parameters for rocks and concrete. Materials and Structures 14, 151–162.

Carpinteri, A., 1982. Notch sensitivity in fracture testing of aggregative materials. Engineering Fracture Mechanics 16, 467–481.

Carpinteri, A., 1987. Stress-singularity and generalized fracture toughness at the vertex of re-entrant corners. Engineering Fracture Mechanics 26, 143–155.

Carpinteri, A., 1989. Cusp catastrophe interpretation of fracture instability. Journal of the Mechanics and Physics of Solids 37, 567–582.

Carpinteri, A., Cornetti, P., Pugno, N., Sapora, A., Taylor, D., 2008. A finite fracture mechanics approach to structures with sharp V-notches. Engineering Fracture Mechanics 75, 1736–1752.

Carpinteri, A., Cornetti, P., Sapora, A., 2011. Brittle failures at rounded V-notches: a finite fracture mechanics approach. International Journal of Fracture 172, 1–8.

Cheng, C.Z., Niu, Z.R., Recho, N., 2012. Effect of non-singular stress on the brittle fracture of V-notched structure. International Journal of Fracture 174, 127–138.

Cornetti, P., Pugno, N., Carpinteri, A., Taylor, D., 2006. Finite fracture mechanics: a coupled stress and energy failure criterion. Engineering Fracture Mechanics 73, 2021–2033.

Cornetti, P., Mantič, V., Carpinteri, A., 2012. Finite fracture mechanics at elastic interfaces. International Journal of Solids and Structures 49, 1022–1032.

Dunn, M.L., Suwito, W., Cunningham, S., 1997a. Fracture initiation at sharp notches: correlation using critical stress intensities. International Journal of Solids and Structures 34, 3873–3883.

Dunn, M.L., Suwito, W., Cunningham, S., May, C.W., 1997b. Fracture initiation at sharp notches under mode I, mode II, and mild mixed mode loading. International Journal of Fracture 84, 367–381.

Dunn, M.L., Suwito, W., Cunningham, S., 1997c. Stress intensities at notch singularities. Engineering Fracture Mechanics 57, 417–430.

Erdogan, F., Sih, G.C., 1963. On the crack extension in plates under plane loading and transverse shear. Journal of Basic Engineering 85, 519–527.

Gómez, F.J., Elices, M., Berto, F., Lazzarin, P., 2009. Fracture of V-notched specimens under mixed mode (I + II) loading in brittle materials. International Journal of Fracture 159, 121–135.

Hasebe, N., Iida, J., 1978. A crack originating from a triangular notch on a rim of a semi-infinite plate. Engineering Fracture Mechanics 10, 773–782.

Hayashi, K., Nemat-Nasser, S., 1981. Energy release rate and crack kinking. International Journal of Solids and Structures 17, 107–114.

Hebel, J., Becker, W., 2008. Numerical analysis of brittle crack initiation at stress concentrations in composites. Mechanics of Advanced Materials and Structures 15, 410–420.

Hebel, J., Dieringer, R., Becker, W., 2010. Modelling brittle crack formation at geometrical and material discontinuities using a finite fracture mechanics approach. Engineering Fracture Mechanics 77, 3558–3572.

Henninger, C., Leguillon, D., Martin, E., 2007. Crack initiation at a V-notch-comparison between a brittle fracture criterion and the Dugdale cohesive model. Comptes Rendu Mécanique 335, 388–393.

Hills, D.A., Dini, D., 2011. Characteristics of the process zone at sharp notch roots. International Journal of Solids and Structures 48, 2177–2183.

Lazzarin, P., Zambardi, R., 2001. A finite-volume-energy based approach to predict the static and fatigue behavior of components with sharp V-shaped notches. International Journal of Fracture 112, 275–298.
Leguillon, D., 2002. Strength or toughness? a criterion for crack onset at a notch. European Journal of Mechanics A/Solids 21, 61–72.
Leguillon, D., Quesada, D., Putot, C., Martin, E., 2007. Prediction of crack initiation at blunt notches and cavities-size effects. Engineering Fracture Mechanics 74, 2420–2436.
Leguillon, D., Piat, R., 2008. Fracture of porous materials – influence of the pore size. Engineering Fracture Mechanics 75, 1840–1853.
Li, J., Zhang, X.B., 2006. Crack initiation prediction for V-notches under mixed-mode loading in brittle materials. Journal of the Mechanics of Materials and Structures 1, 1385–1404.
Livieri, P., Tovo, R., 2009. The use of the $J_V$parameter in welded joints: stress analysis and fatigue assessment. International Journal of Fatigue 31, 153–163.
Mantič, V., 2009. Interface crack onset at a circular cylindrical inclusion under a remote transverse tension. Application of a coupled stress and energy criterion. International Journal of Solids and Structures 46, 1287–1304.
Melin, S., 1994. Accurate data for stress intensity factors at infinitesimal kinks. Journal of applied mechanics 61, 467–470.
Novozhilov, V., 1969. On a necessary and sufficient condition for brittle strength. Journal of Applied Mathematics and Mechanics-USSR 33, 212–222.
Philipps, A.G., Karuppanan, S., Churchman, C.M., Hills, D.A., 2008. Crack tip stress intensity factors for a crack emanating from a sharp notch. Engineering Fracture Mechanics 75, 5134–5139.
Sapora, A., Cornetti, P., Carpinteri, A., 2013. A Finite Fracture Mechanics approach to V-notched elements subjected to mixed-mode loading. Engineering Fracture Mechanics 97, 216–226.
Seweryn, A., 1994. Brittle fracture criterion for structures with sharp notches. Engineering Fracture Mechanics 47, 673–681.
Seweryn, A., Poskrobko, S., Mroz, Z., 1997. Brittle fracture in plane elements with sharp notches under mixed-mode loading. Journal of Engineering Mechanics-ASCE 123, 535–543.
Seweryn, A., Lukaszewicz, A., 2002. Verification of brittle fracture criteria for elements with V-shaped notches. Engineering Fracture Mechanics 69, 1487–1510.
Sinclair, G., Okajima, M., Griffin, J., 1984. Path independent integrals for computing stress intensity factors at sharp notches in elastic plates. International Journal of Numerical Methods in Engineering 20, 999–1008.
Strandberg, M., 2002. Fracture at V-notches with contained plasticity. Engineering Fracture Mechanics 69, 403–415.
Taylor, D., 2007. The Theory of Critical Distances: A New Perspective in Engineering Fracture Mechanics. Elsevier, Oxford.
Weißgraeber, P., Becker, W., 2011. Predicting effective strengths of bonded lap joints with a finite fracture mechanics criterion. In: Proceedings of the 32nd Risø International Symposium in Materials Science "Composite materials for structural performance: Towards higher Limits", pp. 479–486.
Williams, M.L., 1952. Stress singularities resulting from various boundary conditions in angular corners of plates in extension. Journal of Applied Mechanics 74, 526–528.
Wu, C.H., 1978. Maximum energy release rate criterion applied to a tension–compression specimen with crack. Journal of Elasticity 8, 235–257.
Yosibash, Z., Adan, O., Shneck, R., Atlas, H., 2003. Thermomechanical failure criterion at the micron scale in electronic devices. International Journal of Fracture 122, 47–64.
Yosibash, Z., Priel, E., Leguillon, D., 2006. A failure criterion for brittle elastic materials under mixed-mode loading. International Journal of Fracture 141, 291–312.